

5-2018

Differential Launch Structures and Common Mode Filters for Planar Transmission Lines

Zachary Thomas Bergstedt

Follow this and additional works at: https://scholar.rose-hulman.edu/electrical_grad_theses



Part of the [Electrical and Electronics Commons](#)

Recommended Citation

Bergstedt, Zachary Thomas, "Differential Launch Structures and Common Mode Filters for Planar Transmission Lines" (2018).
Graduate Theses - Electrical and Computer Engineering. 9.
https://scholar.rose-hulman.edu/electrical_grad_theses/9

This Thesis is brought to you for free and open access by the Graduate Theses at Rose-Hulman Scholar. It has been accepted for inclusion in Graduate Theses - Electrical and Computer Engineering by an authorized administrator of Rose-Hulman Scholar. For more information, please contact weir1@rose-hulman.edu.

Differential Launch Structures and Common Mode Filters for Planar Transmission Lines

A Thesis

Submitted to the Faculty

of

Rose-Hulman Institute of Technology

by

Zachary Thomas Bergstedt

In Partial Fulfillment of the Requirements for the Degree

of

Master of Science in Electrical Engineering

May 2018

© 2018 Zachary Thomas Bergstedt



ROSE-HULMAN INSTITUTE OF TECHNOLOGY

Final Examination Report

Zachary Bergstedt

Name

Electrical Engineering

Graduate Major

Thesis Title Differential Launch Structures and Common Mode Filters for Planar Transmission Lines

DATE OF EXAM:

April 25, 2018

EXAMINATION COMMITTEE:

Thesis Advisory Committee		Department
Thesis Advisor:	Edward Wheeler	ECE
	JianJian Song	ECE
	Azad Siahmakoun	PHOE
	Michael Cracraft	IBM

PASSED

 x

FAILED

ABSTRACT

Bergstedt, Zachary Thomas

M.S.E.E.

Rose-Hulman Institute of Technology

May 2018

Differential Launch Structures and Common Mode Filters for Planar Transmission Lines

Thesis Advisor: Dr. Edward Wheeler

Increases in signal speeds and decreases in dimensions pose increasing threats to signal integrity (SI) and electromagnetic compatibility (EMC) in differential interconnects due to the enhanced risk of common mode (CM) conversion. This thesis examines CM filtering solutions for multiple transmission topologies that mitigate CM noise, reducing the threat to SI and EMC. These topologies include microstrip and stripline, which are the most commonly used transmission line architecture in printed circuit boards (PCB), and broadside coupled coplanar waveguides (BC-CPW). Stripline and BC-CPW transmission lines have lower dispersion and attenuation than the commonly used microstrip but have added complexity in introducing the signal to the transmission line in a PCB environment. Differential signal launches are introduced that maintain differential transmission from DC to 20 GHz with less than -8 dB of common mode conversion and better than -3.5 dB.

Keywords:

TABLE OF CONTENTS

LIST OF FIGURES	iii
LIST OF TABLES	v
LIST OF ABBREVIATIONS	vi
LIST OF SYMBOLS	vii
GLOSSARY	viii
1. INTRODUCTION	1
2. BACKGROUND	3
2.1. Even and Odd Mode Transmission Line Characteristics	3
2.2. Mixed-mode Transmission Line Characteristics	6
2.3. Differential Transmission	7
2.4. Scattering Parameters.....	9
3. LITERATURE REVIEW	13
3.1. Mode-Selective Transmission Lines and Their Relationship To Common Mode Filtering	13
3.2. Common Mode Filtering Structures	15
4. A MODEL FOR COMMON MODE FILTERING	18
4.1. Quarter Wavelength Resonator	18
4.2. Common Mode Filtering in Microstrip Environments	18
4.3. Common Mode Filtering in Stripline Environments	20
4.4. Common Mode Filtering in Broadside Coupled CPW	22
4.5. Differential Launch Structure for a Stripline Environment	24
4.6. Differential Launch Structure for Broadside Coupled Coplanar Waveguide	27
5. FILTER AND LAUNCH STRUCTURE DESIGN AND VALIDATION	30
5.1. Microstrip Filtering Structures.....	33
5.2. Stripline Launch Structures and Filters.....	34
5.3. Broadside Coupled Coplanar Waveguide Launch Structure and Filters.....	38
6. PERFORMANCE AND DISCUSSION OF LAUNCH STRUCTURES AND FILTERS	46
6.1. Stripline and Broadside Coupled Coplanar Waveguide Launch Structures	47
6.2. Microstrip Filter Performance.....	53
6.3. Stripline Filter Performance.....	57
6.4. Broadside Coupled Coplanar Waveguide Filter Performance	58

7. LIMITATIONS	64
8. FUTURE WORK	66
9. CONCLUSION	69
REFERENCES	70
APPENDICES	71
Appendix A: Single-Ended to Mixed-Mode S-Parameter Conversions	71
Appendix B: Test Board Models and Pictures.....	72
Appendix C: S-Parameter Results for All Filter Structures	74

LIST OF FIGURES

<u>Figure 2.1: Three-Wire Transmission Line Network</u>	5
<u>Figure 2.2: Odd-Mode Excitation of a Three Wire Transmission Line Network</u>	6
<u>Figure 2.3: Asymmetry in Coupled Transmission Lines</u>	8
<u>Figure 2.4: Four-port Coupled Transmission Lines</u>	9
<u>Figure 3.1: Mode-Selective Transmission Line Architecture</u>	14
<u>Figure 3.2: Differential Mode-Selective Transmission Line Architecture</u>	15
<u>Figure 3.3: Typical Common Mode Filtering Structures</u>	16
<u>Figure 3.4: Flux Structures in a Defected Ground Plane Filter</u>	17
<u>Figure 4.2: Microstrip Bowtie Filter</u>	19
<u>Figure 4.3: Stripline Cross Section</u>	21
<u>Figure 4.4: Stripline Bowtie Filter</u>	22
<u>Figure 4.5: Broadside Coupled Coplanar Waveguide Bowtie Filter</u>	23
<u>Figure 4.6: Stripline Transition</u>	25
<u>Figure 4.7: Broadside Coupled Coplanar Waveguide Transition</u>	28
<u>Figure 5.1: Mixed-Mode S-Parameter Measurement Setup</u>	32
<u>Figure 5.2: Bowtie Filter Structures Implemented in Microstrip</u>	33
<u>Figure 5.3: Stripline Launch Structure Dimensions</u>	35
<u>Figure 5.4: Bowtie Filter Structures Implemented in Stripline</u>	37
<u>Figure 5.5: BC-CPW Launch Structure Dimensions</u>	38
<u>Figure 5.6: Bowtie Filter Structures Implemented in BC-CPW</u>	43
<u>Figure 6.1: BC-CPW Launch Structure S-Parameter Results</u>	47
<u>Figure 6.2: BC-CPW Time Domain Reflectometer Measurement Results</u>	49
<u>Figure 6.3: Stripline Launch Structure S-Parameter Results</u>	51
<u>Figure 6.4: Microstrip Filtering Structure S-Parameter Results</u>	54
<u>Figure 6.5: Stripline Filtering Structure S-Parameter Results</u>	58
<u>Figure 6.6: BC-CPW 11 GHz Filtering Structure S-Parameter Results</u>	59

<u>Figure 6.7: BC-CPW Cascaded Filtering Structures S-Parameter Results</u>	60
<u>Figure 6.8: BC-CPW Asymmetric Filtering Structure S-Parameter Results</u>	60
<u>Figure 6.9: BC-CPW RF Probe Launched Filter S-Parameter Results</u>	61
<u>Figure B.1: Test Board Overview</u>	72
<u>Figure C.1: Microstrip 3 Cascaded Symmetric Filters S-Parameter Results</u>	74
<u>Figure C.2: Microstrip 2 Cascaded Symmetric Filters S-Parameter Results</u>	74
<u>Figure C.3: Microstrip Single Asymmetric Filter S-Parameter Results</u>	75
<u>Figure C.4: Stripline Single Symmetric 5 GHz Filter S-Parameter Results</u>	76
<u>Figure C.5: Stripline Single Symmetric 8 GHz Filter S-Parameter Results</u>	76
<u>Figure C.6: Stripline Single Symmetric 16 GHz Filter S-Parameter Results</u>	77
<u>Figure C.7: Stripline 3 Cascaded Symmetric Filters S-Parameter Results</u>	77
<u>Figure C.8: BC-CPW Single Symmetric 8 GHz Filter S-Parameter Results</u>	78
<u>Figure C.9: BC-CPW Single Symmetric 11 GHz Filter S-Parameter Results</u>	78
<u>Figure C.10: BC-CPW Single Symmetric 16 GHz Filter S-Parameter Results</u>	79
<u>Figure C.11: BC-CPW 3 Cascaded Symmetric Filters S-Parameter Results</u>	79
<u>Figure C.12: BC-CPW 2 Cascaded Symmetric Filters S-Parameter Results</u>	80
<u>Figure C.13: BC-CPW Single Asymmetric Filter S-Parameter Results</u>	80
<u>Figure C.14: BC-CPW RF Probe 3 Cascaded Symmetric Filters S-Parameter Results</u>	81
<u>Figure C.15: BC-CPW RF Probe 2 Cascaded Symmetric Filters S-Parameter Results</u>	81
<u>Figure C.16: BC-CPW RF Probe Single Asymmetric Filters S-Parameter Results</u>	82

LIST OF TABLES

Table 5.1: Microstrip Filter Dimensions.....	34
Table 5.2: Stripline Launch Dimensions	36
Table 5.3: Stripline Filter Dimensions.....	37
Table 5.4: BC-CPW Launch Dimensions.....	42
Table 5.5: BC-CPW Filter Dimensions	45
Table B.1: Test Board Overview	73

LIST OF ABBREVIATIONS

BC-CPW	Broadside Coupled Coplanar Waveguide
CM	Common Mode
CPW	Coplanar Waveguide
DM	Differential Mode
EMC	Electromagnetic Compatibility
MSTL	Mode Selective Transmission Line
PCB	Printed Circuit Board
SI	Signal Integrity

LIST OF SYMBOLS

λ	Wavelength
Z_c	Characteristic Impedance
C	Capacitance
V	Voltage
I	Current
a	Incoming power wave
b	Outgoing power wave
S_{ij}	Scattering parameter from port j to port i
ϵ	Relative permittivity
v_p	Electromagnetic propagation velocity
c	The propagation velocity of light in free space
Ω	Ohms

GLOSSARY

Wave Number - a parameter of how much the phase of a progresses in a unit of distance

Common Mode - a mode of energy when two excitations have the same amplitude and direction

Differential Mode - a mode of energy when two excitations have the same amplitude and opposite directions

Signal Integrity - the input signal reaches the output port

Electromagnetic Compatibility - the lack of interference from one region of a circuit with another region of a circuit, whether the same circuit or a different one

Characteristic Impedance - the ratio relating the voltage and current in a transmission line

1. INTRODUCTION

Differential mode signaling is often used in high speed interconnects to mitigate noise and crosstalk. This becomes more difficult with continuing increases in signal speeds and shrinking dimensions, which represent twin challenges to the limits of existing interconnect technology. The presence of common mode conversion, when differential mode energy is converted to common mode energy, represents a significant threat to the electromagnetic compatibility (EMC) and signal integrity (SI) environment of printed circuit boards (PCBs), a challenge which grows more serious as frequencies continue to increase and the wavelengths shrink. Common mode (CM) filtering solutions exist to mitigate the presence of CM noise but may be unsuitable due to their lack of effectiveness, their frequency limitations, or their added complexity and cost.

A critical enabling technology and an area overlooked in research investigations is signal launch. A practical signal launch, offering high-performance over a wide range of frequencies is critical if the CM filtering structures are ever going to be used in applications and in commercial products. Whatever the topology of the differential communication link and its associated CM filtering structure is, effective signal launches must be brought to one side of the PCB since modern integrated circuit use a ball-grid array to make electrical contact to the host PCB. Regardless of the CM filtering solution's effectiveness, their utility will be limited without signal launches providing access to the structures on a single side of a PCB. The signal launch is therefore crucial, and its performance must be such that it remains effective over a broad range of frequencies, a difficult task at microwave and mm-wave frequencies.

In work reported here, signal launches are designed for coplanar waveguide (CPW) based structures, which rely on broadside coupling to form differential communication links, and also for stripline based structures with edge coupling. Both CPW and stripline show effective

transmission through mm-range wavelengths. This can be contrasted with microstrip based structures which display significant loss (largely due to radiation) at higher frequencies.

2. BACKGROUND

In order to analyze the filters and launch structures, an understanding of even and odd mode analysis, common and differential mode transmission, and single-ended and mixed-mode scattering parameters (S-parameters) is needed. In particular, mixed-mode S-parameters and their relationship to single-ended S-parameters are important to understand. Single-ended S-parameters are what is measured and mixed-mode S-parameters are what is used to characterize the differential transmission line network.

2.1. Even and Odd Mode Transmission Line Characteristics

Electromagnetic energy propagates as waves, in free space as “plane waves,” so-called since their surfaces of constant phase form planes. These waves can be characterized by the intrinsic impedance of the medium, η , and the wave number, β . The intrinsic impedance is the ratio of magnitudes between the electric and magnetic fields, and the wavenumber is inversely related to the wavelength and is the number of waves in 2π meters. In free space, the wave number is related to wavelength by the following equation.

$$\beta = \frac{2\pi}{\lambda} = 2\pi f \sqrt{\mu\epsilon} \quad (2.1)$$

and the intrinsic impedance is related to permittivity, ϵ , and permeability, μ , by the following equation.

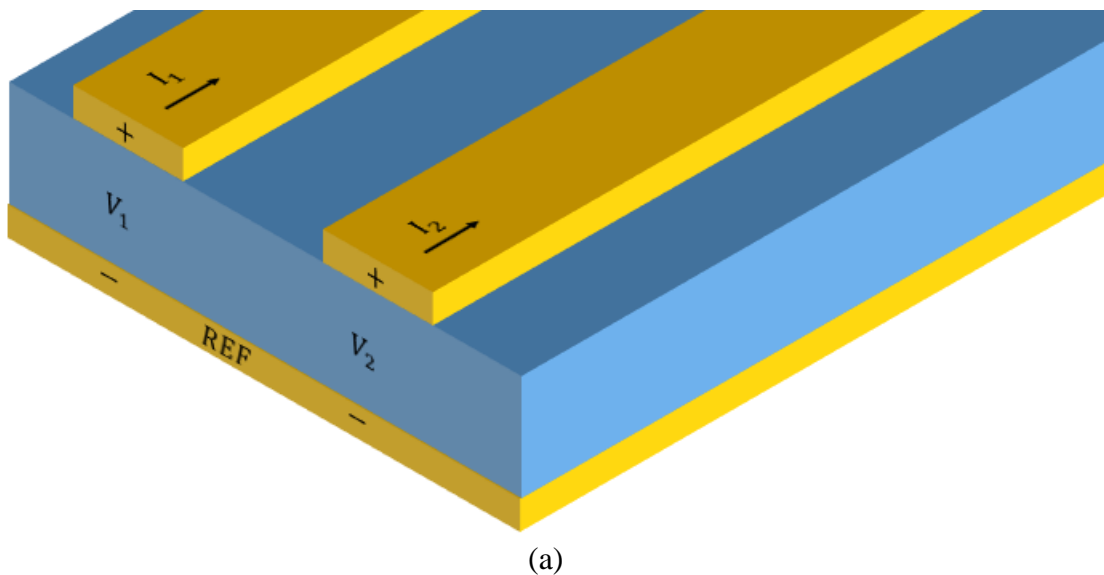
$$\eta = \sqrt{\frac{\mu}{\epsilon}} \quad (2.2)$$

These two parameters characterize the propagation of the wave. In transmission lines, Maxwell’s equations can be simplified by allowing the use of transmission line equations which are expressed in terms of voltages and currents. The voltage is obtained with a line integral of the electric field from one conductor to another, and the current is obtained by finding the

circulation of the magnetic field about a conductor. In transmission lines, the waves can be characterized similarly by the characteristic impedance, Z_c , which includes the geometry and electric and magnetic materials of the media in the transmission line. The characteristic impedance can be expressed in terms of L and C , the transmission line's per-unit-length (PUL) inductance and capacitance.

$$Z_c = \sqrt{\frac{L}{C}} \quad (2.3)$$

With the basis of a single transmission line, we can start to analyze two coupled transmission lines. In most cases, these coupled lines consist of two transmission lines with a single reference plane, though there may be multiple reference planes that are at the same potential. As a circuit, this can be modeled as shown in Fig. 2.1(b) [1], where C_{11} represents the capacitance between trace 1 and reference, C_{12} represents the capacitance between traces, and C_{22} represents the capacitance between trace 2 and ground. The inductance, L , is not affected as strongly as capacitance, and will not be considered. Assuming the traces are identical, $C_{11} = C_{22}$.



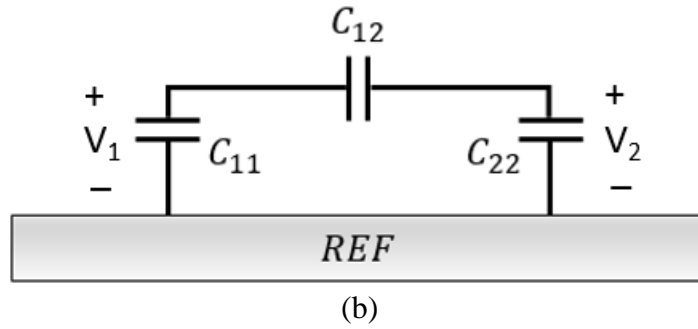


Fig. 2.1 - (a) Three-wire transmission line network and (b) the equivalent capacitance network

With this model, consider an even mode excitation, where the currents in the traces are equal in amplitude and direction and consider an odd mode excitation, where the currents in the traces are equal in amplitude but in opposite directions. Correspondingly, in the even mode, $V_1 = V_2$ and in the odd mode, $V_1 = -V_2$. In the even mode, there will be no current through C_{12} which can be replaced by an open circuit. Because of this, the capacitance from either line in the even mode, C_e , will just equal C_{11} or C_{22} . The characteristic impedance will then be equal to

$$Z_{ce} = \sqrt{\frac{L}{C_e}} \quad (2.4)$$

In the odd mode excitation, the flux pattern will be odd symmetric about a plane in the center between the two traces. In the circuit model, this can be treated as a ground plane between the two capacitances as shown in Fig. 2.2(b) [1].

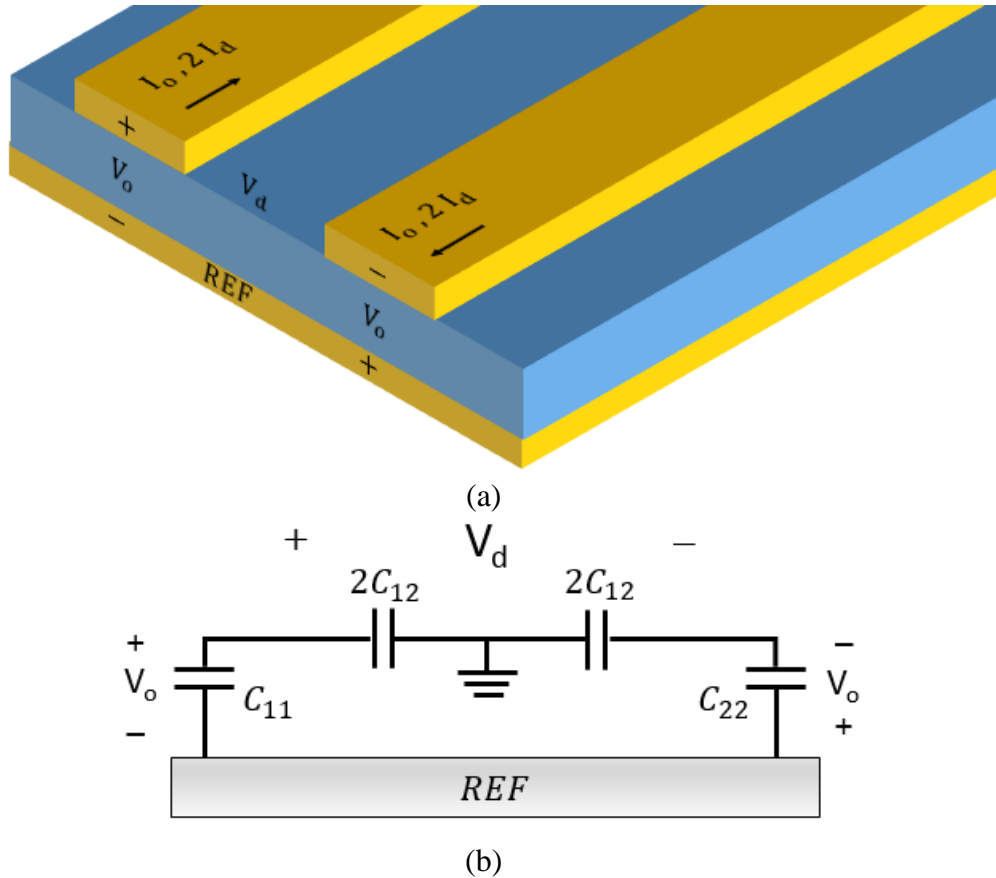


Fig. 2.2 - (a) Three wire transmission line network with an odd mode excitation and (b) the equivalent capacitance network

The effective capacitance in the odd mode, C_o will then be

$$C_o = C_{11} + 2C_{12} = C_{22} + 2C_{12} \quad (2.5)$$

and the characteristic impedance is

$$Z_{co} = \sqrt{\frac{L}{C_o}} \quad (2.6)$$

Any excitation of a three conductor network can be treated as a superposition of these even and odd mode excitations.

2.2. Mixed-mode Transmission Line Characteristics

Using even and odd mode analysis, we can express an excitation on trace 1 and trace 2 as

$$V_1 = \frac{V_e + V_o}{2} \quad (2.7)$$

$$V_2 = \frac{V_e - V_o}{2} \quad (2.8)$$

respectively [2]. The average or common mode voltage will be

$$V_c = \frac{V_1 + V_2}{2} \quad (2.9)$$

and the difference or differential mode voltage will be

$$V_d = V_1 - V_2 \quad (2.10)$$

Similarly, the currents will be

$$I_c = I_1 + I_2 \quad (2.11a)$$

$$I_d = \frac{I_1 - I_2}{2} \quad (2.11b)$$

Using these definitions, the common and differential mode impedances will thus be

$$Z_{cc} = \frac{1}{2} \frac{V_1 + V_2}{I_1 + I_2} = \frac{1}{2} Z_{ce} \quad (2.12a)$$

$$Z_{cd} = 2 \frac{V_1 - V_2}{I_1 - I_2} = 2 Z_{co} \quad (2.12b)$$

2.3. Differential Transmission

Differential mode signaling has several advantages over single-ended signaling and is commonly used in digital interconnects. In pure differential signaling, there will be no net current through any cross section that surrounds both traces, so unwanted radiation and subsequent electromagnetic interference (EMI) will be reduced. In the near-field, crosstalk is reduced through reduced net electric and magnetic coupling. Additionally, any DC offset will be canceled out and the effects of noise may be reduced due to the close proximity that results in a correlation of the noise, which will also be canceled out.

Common mode energy can cause reduced immunity and increase crosstalk and radiation, and so poses a serious threat to a system's EMC and SI environment. Common mode conversion, where some DM energy is converted to CM, occurs when there is asymmetry in the environment, most often unequal capacitive coupling of the two traces to the reference, of the two lines forming the differential link, or when the electrical length of the two differential transmission lines is unequal resulting in skew. It can also be present in the initial signaling due to imperfections in the signal source such as in cases when the rise and fall times of the signal are not the same.

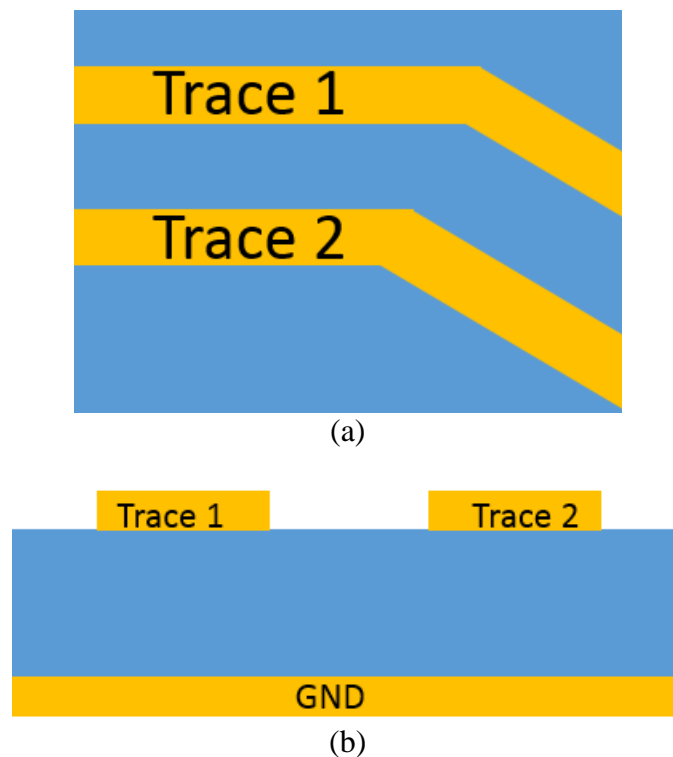


Fig. 2.3 - Coupled transmission lines with asymmetry from a bend in the line (a) top view and (b) cross section

To illustrate, consider a differential transmission line comprising two microstrip transmission lines as shown in Fig. 2.3. The differential transmission lines are formed by coupling two transmission lines. To distinguish these lines from the differential transmission

line they form, they are usually referred to as “single-ended” lines so that two coupled single-ended lines form a differential transmission line. As seen in Fig. 2.3, a bend in the signal path results in one line becoming longer than the other, introducing skew which could result in CM conversion and its attendant negative effects.

2.4. Scattering Parameters

The microstrip-based differential transmission line shown above can be considered a four-port (four single-ended ports, that is) network as illustrated in Fig. 2.4. The port parameters used at microwave and mm-wave signals are described in terms of power waves, which are proportional to the square root of the wave’s power. Power waves directed toward the ports are denoted as a_1, a_2, \dots, a_N referring the waves going into ports 1, 2, \dots , N. Similarly, power waves leaving the ports are denoted as b_1, b_2, \dots, b_N

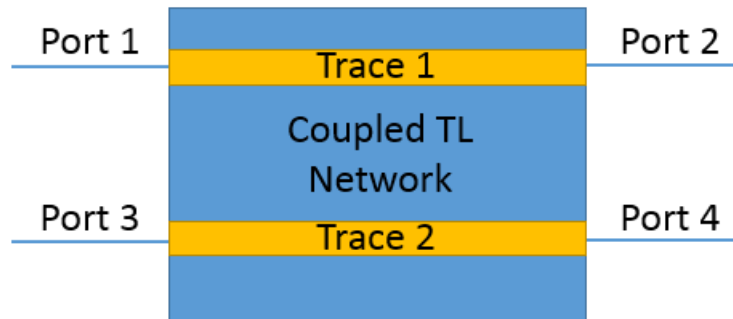


Fig. 2.4 - Coupled TL network as a four-port device

Power waves are defined as

$$a = \frac{V + Z_c I}{2\sqrt{Z_c}} = \frac{V^+}{\sqrt{Z_c}} \quad (2.13a)$$

$$b = \frac{V - Z_c I}{2\sqrt{Z_c}} = \frac{V^-}{\sqrt{Z_c}} \quad (2.13b)$$

where a is the incident power wave, and b is the reflected or outgoing power wave. V^+ and V^- are the incident and outgoing voltage waves respectively [1]. Similarly to voltages, power waves can likewise be defined for differential mode and common mode.

$$a_d = \frac{V_d + Z_{cd}I_d}{2\sqrt{Z_{cd}}} \quad (2.14a)$$

$$a_c = \frac{V_c + Z_{cc}I_c}{2\sqrt{Z_{cc}}} \quad (2.14b)$$

$$b_d = \frac{V_d - Z_{cd}I_d}{2\sqrt{Z_{cd}}} \quad (2.14c)$$

$$b_c = \frac{V_c - Z_{cc}I_c}{2\sqrt{Z_{cc}}} \quad (2.14d)$$

Using these power waves, it is more convenient to think of the two single-ended ports 1 and 3 as forming a differential port 1 with both positive and negative-going differential mode and common mode signals. Likewise one can consider single-ended ports 2 and 4 as forming differential port 2 again with both positive and negative-going differential mode and common mode signals. Assuming differential port 1 is comprised of single-ended ports 1 and 3 and differential port 2 is comprised of single-ended ports 2 and 4, equations (2.9)-(2.12b) and equations (2.14a-d) can be used to determine the relationship between these so-called mixed-mode waves and single-ended power waves to be

$$a_{d1} = \frac{a_1 - a_3}{\sqrt{2}} \quad (2.15a)$$

$$a_{c1} = \frac{a_1 + a_3}{\sqrt{2}} \quad (2.15b)$$

$$b_{d1} = \frac{b_1 - b_3}{\sqrt{2}} \quad (2.15c)$$

$$b_{c1} = \frac{b_1 + b_3}{\sqrt{2}} \quad (2.15d)$$

At mixed-mode port 2, single-ended ports 2 and 4 are substituted for ports 1 and 3.

Scattering parameters are defined relative to the incident and reflected power waves. Let us first consider the relationship between single-ended signals.

$$\begin{bmatrix} b_1 \\ \vdots \\ b_N \end{bmatrix} = \begin{bmatrix} S_{11} & \cdots & S_{1N} \\ \vdots & \ddots & \vdots \\ S_{N1} & \cdots & S_{NN} \end{bmatrix} \begin{bmatrix} a_1 \\ \vdots \\ a_N \end{bmatrix} \quad (2.16)$$

A specific element in the scattering matrix can be found as

$$S_{ij} = \left. \frac{b_i}{a_j} \right|_{a_k=0 \text{ for } k \neq j} \quad (2.17)$$

where b_i is the voltage reflected or directed in the outgoing direction at the i th port and a_i is the input voltage or the voltage going into the device at the j th port. For a four-port device, there will be sixteen elements in the 4 x 4 scattering matrix. Using this relationship and the relationships between single-ended and mixed-mode power waves from equations (2.15a-b), mixed-mode scattering parameters can be derived from single-ended parameters.

In the common mode, $a_1 = a_3$ and in the differential mode, $a_1 = -a_3$. Using the scattering parameter relationship, the outgoing voltages at each port can be determined for common and differential mode excitations.

$$\begin{bmatrix} b_1 \\ b_2 \\ b_3 \\ b_4 \end{bmatrix} = \begin{bmatrix} S_{11} & S_{13} \\ S_{21} & S_{23} \\ S_{31} & S_{33} \\ S_{41} & S_{43} \end{bmatrix} \begin{bmatrix} a_1 \\ a_3 \end{bmatrix} \quad (2.18)$$

Mixed-mode scattering parameters are evaluated the same as single-ended scattering parameters except the mode is included. For example, if the excitation is differential mode at mixed-mode

port 1 and the received signal is at mixed-mode port 2 in common mode, the scattering parameter would be calculated as

$$S_{cd21} = \left. \frac{b_{c2}}{a_{d1}} \right|_{a_{ck}=a_{dk}=0 \text{ for } k \neq 1} = \left. \frac{b_2 + b_4}{a_1 - a_3} \right|_{a_1 = -a_3, a_k = 0 \text{ for } k \neq 1,3} \quad (2.19)$$

The reflected power waves can then be related to the incident power waves using single-ended scattering parameters using equation (2.18). Additionally, the incident power waves can be related because of the mode. This yields

$$S_{cd21} = \frac{(S_{21} - S_{23})a_1 + (S_{41} - S_{43})a_1}{2a_1} = \frac{1}{2}(S_{21} - S_{23} + S_{41} - S_{43}) \quad (2.20)$$

This derivation can be repeated for each combination of input and output port and mode. The most useful equations are given below. The rest are included in Appendix A.

$$\text{Differential Mode Reflection: } S_{dd11} = 1/2 (S_{11} - S_{13} - S_{31} + S_{33}) \quad (2.21a)$$

$$\text{Differential Mode Reflection: } S_{dd21} = 1/2 (S_{21} - S_{41} - S_{23} + S_{43}) \quad (2.21b)$$

$$\text{Common Mode Conversion: } S_{cd21} = 1/2 (S_{21} + S_{41} - S_{23} - S_{43}) \quad (2.21c)$$

$$\text{Common Mode Transmission: } S_{cc21} = 1/2 (S_{11} + S_{13} + S_{31} + S_{33}) \quad (2.21d)$$

3. LITERATURE REVIEW

Existing solutions for differential transmission may be inadequate for mm-wave applications. Existing differential transmission line architectures have limited coupling between the differential traces, limiting the benefits of using the differential transmission in the first place, and loss and dispersion that becomes prohibitive in the mm-wave range. Existing common mode filtering structures either require a shared, broadside coupled ground plane or are bandpass filters that cannot accommodate wideband differential signals.

3.1. Mode-Selective Transmission Lines and Their Relationship To Common Mode Filtering

Limitations exist in stripline and microstrip transmission lines due to their dispersion and attenuation at high frequencies. These architectures are adequate at low frequencies, and solutions exist for propagation at high frequency. What is lacking is a transmission line architecture able to accommodate wideband signals such as picosecond pulses which have frequency components extending from DC to millimeter wave frequencies. A new architecture was introduced in [3] called mode-selective transmission lines (MSTL) that has low dispersion and attenuation both at low frequencies and at millimeter wave frequencies. In this architecture, the top metal layer is a coplanar waveguide with vias connecting the coplanar reference with the bottom reference layer as shown in Fig. 3.1. Careful design allows these vias to act as walls for a surface integrated waveguide at high frequencies.

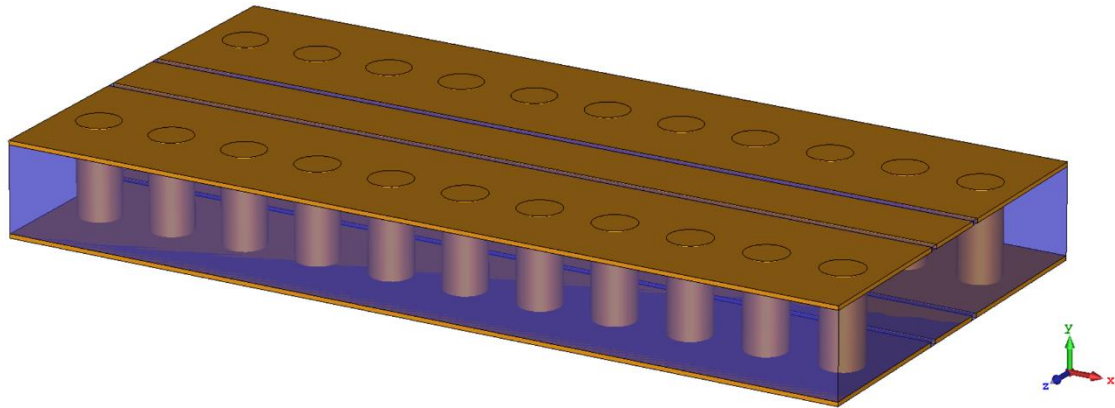


Fig. 3.1 - Mode-selective transmission line architecture

At low frequencies, the architecture has the flux pattern of a microstrip transmission line. This is the TEM mode of operation where most of the flux is coupled from the microstrip line to the ground plane. As the frequency increases, the flux becomes less confined to the microstrip pattern and the TEM mode. Eventually, the TE_{10} mode dominates. In this mode, the electric field spreads out to the via fence walls, approximating a rectangular waveguide.

This architecture is attractive for differential transmission and common mode filtering due to its potential for symmetry that will not affect differential mode impedance but will alter common mode impedance. Indeed, the earlier work by Ke Wu's group [3] on these single-ended structures was the original motivation for all the CPW-based structures shown here. If the transmission line is mirrored across the ground plane, as depicted in Fig. 3.2(a), the middle ground plane will isolate the two transmission lines. This topology will be referred to as broadside coupled coplanar waveguide (BC-CPW).

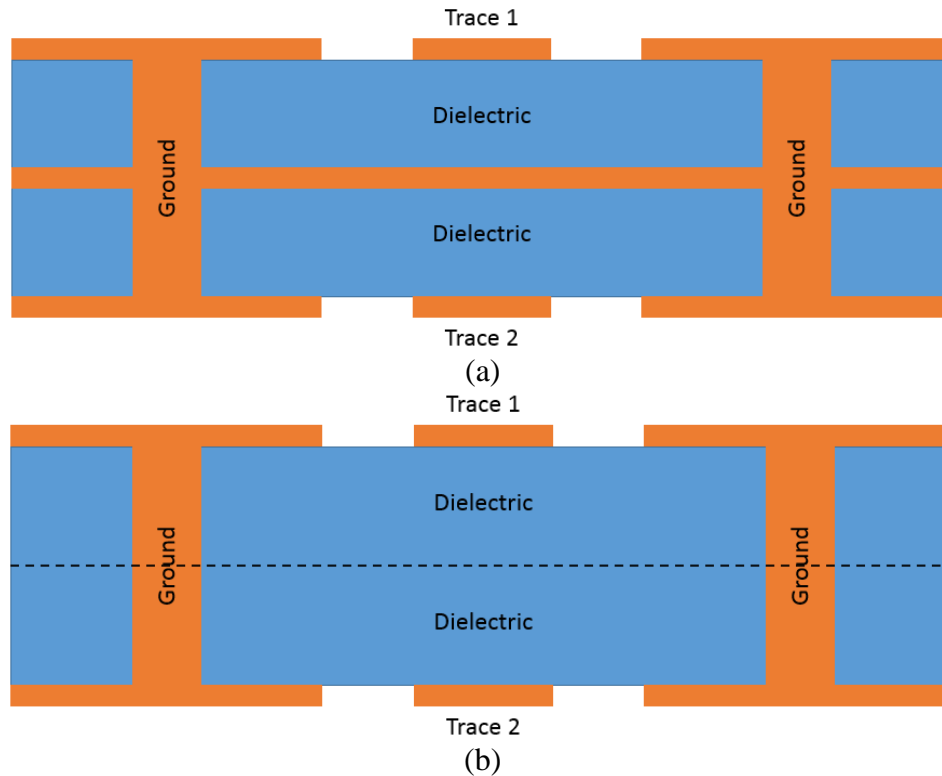


Fig. 3.2 - Mirrored mode-selective transmission line (a) with center reference plane and (b) without center reference plane

As discussed in Section 2.1, a virtual ground can be placed in the center plane between the differential traces for TEM modes. This means that removing the center ground plane will have no effect on the differential mode impedance. In common mode, the center line is replaced by a magnetic ground, resulting in a drastically different impedance and flux structures with and without the center reference layer. This characteristic is very attractive for common mode filtering and because filtering structures placed in the center reference layer is likely to affect common mode transmission much more strongly than differential mode.

3.2. Common Mode Filtering Structures

Options currently exist for common mode filtering structures. The two most common types of common mode filters are defected ground plane structures [4, 5, 6, 7, 8] and balanced filters

[4, 9, 10, 11]. Defected ground plane filters rely on net electric flux into the filter in common mode and no net electric flux into the filter in differential mode, while balanced filters rely on the symmetry of common mode versus the antisymmetry of differential mode.

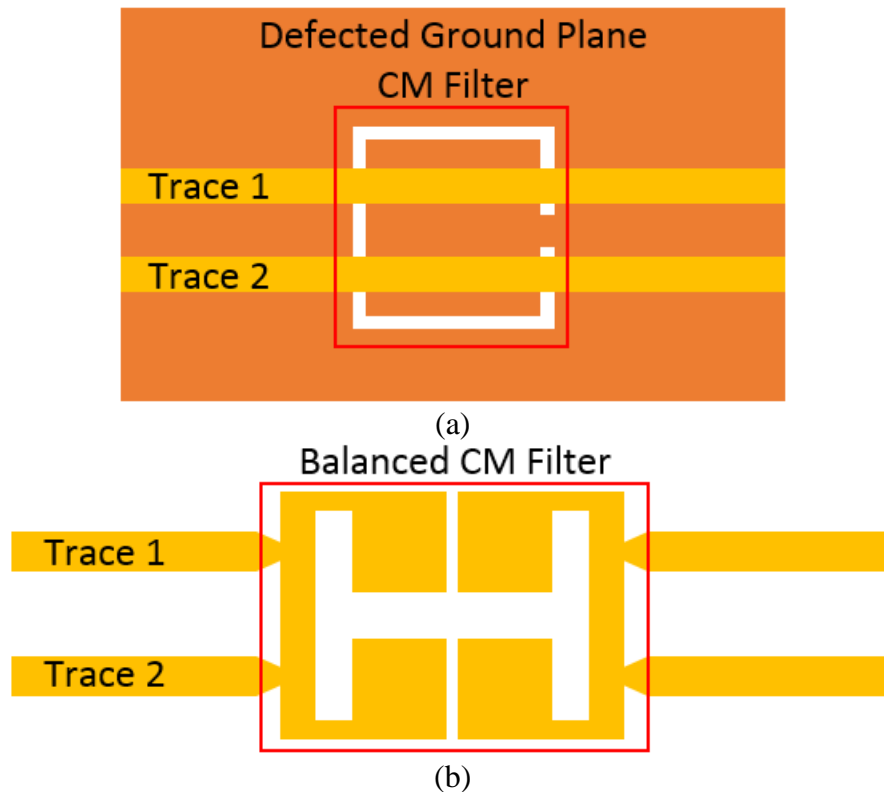


Fig. 3.3 - Typical Common Mode filtering structures utilizes a (a) defected ground plane and a (b) balanced bandpass filter

Defected ground plane filters consist of resonators embedded in the ground plane below the differential transmission lines as in Fig. 3.3(a). In common mode, there is net flux into the resonator, exciting it and hampering common mode transmission. In differential mode, there is electric flux coupling into the resonator from one trace and electric flux coupling out of the resonator to the other trace. The result is approximately zero net flux to the reference in the differential mode, resulting in very little or no attenuation in differential mode transmission.

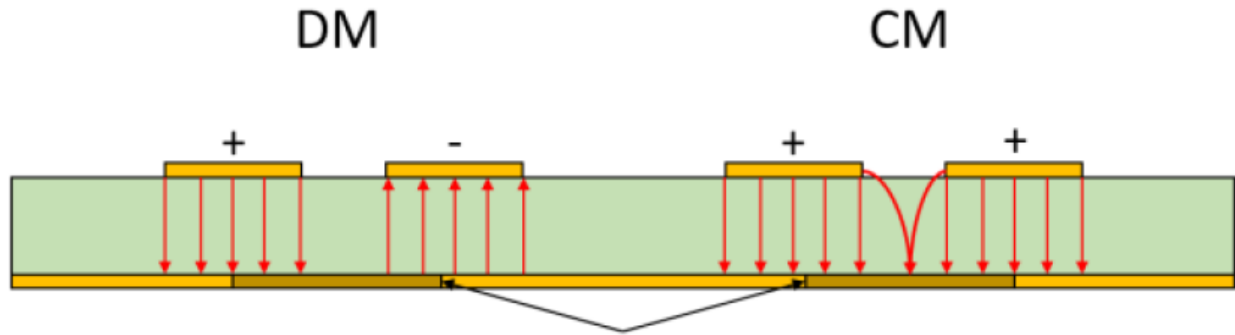


Fig. 3.4 - DM and CM flux patterns of a differential microstrip pair with defected ground plane

Balanced filters generally consist of a filter structure that is connected to both traces. The balanced filter is often a single-ended filter mirrored about the center plane between the coupled traces as in Fig. 3.3(b). With the symmetry of common mode, the combined filter acts as a bandstop filter. With the antisymmetry of differential mode, the combined filter acts as a bandpass filter where the differential pass band is the same as the common mode stop band.

Both filter types have their advantages. Defected ground plane structures are compact and do not take up much space since they are in the ground plane which has to be there anyway. Balanced filters double as bandpass filters and can have extremely high common mode rejection ratios. However, both these filter types have drawbacks. They are nearly all designed for edge-coupled microstrip transmission lines. They can be adapted to other transmission line topologies like stripline but may have limited effectiveness and increased complexity. Additionally, defected ground plane structures they are not easily adaptable to topologies like coplanar waveguides where there is not a shared broadside coupled ground plane. Defected ground plane filters are incompatible with the previously proposed BC-CPW topology for this reason and because there will be no net electric flux through the center plane in common mode and net flux in differential mode.

4. A MODEL FOR COMMON MODE FILTERING

The CM filtering structure examined here is useful primarily due to its simplicity and adaptability. The quarter wavelength resonator has an uncomplicated design equation and can be implemented in almost any differential topology. Practical use in stripline and BC-CPW architectures require launch structures which are also considered below.

4.1. Quarter Wavelength Resonator

If a length of transmission line with a short at the end is placed in parallel as a stub with a transmission line, it will act as a bandpass filter where the passband occurs when the length of the stub is a quarter of the wavelength [1]. Conversely, if the short-circuited stub were placed in series with transmission line, it would act as a notch filter, passing all frequencies except for where the length is a quarter of the wavelength. This notch filter can be accomplished through the use of a coupled line filter. Instead of the resonator directly touching the transmission line, it is coupled to the transmission line. It can be shown through even and odd mode analysis that this will result in a notch filter as if the resonator were in series with the transmission line [1]. Since the filter is excited by the electric flux of the transmission lines and the flux patterns of common mode and differential mode signals are different, this filter can be implemented to only affect the common mode transmission and not significantly impact the differential mode transmission.

4.2. Common Mode Filtering in Microstrip Environments

Microstrip is one of the simplest architectures for transmission lines. It is simply a single trace of copper above a ground plane. Since it is on the outer layer of the board, it requires no transmission to link to a connector or component. Its simplicity and low-cost combine to make it

a common architecture. CM filtering can be accomplished by putting a bowtie filter in the middle of the two coupled microstrip traces as in Fig. 4.2. This addition will have a small effect on the differential impedance due to the non-ideality and finite size of the filter.

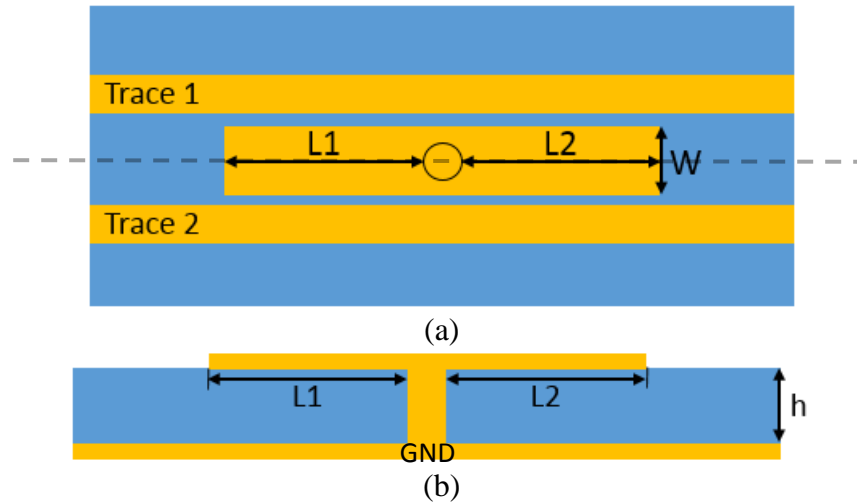


Fig. 4.2 - Bowtie filtering structure between microstrip traces (a) top view and (b) cross section cut at the dotted line

The filter will attenuate most strongly when

$$L1 + h = \frac{\lambda}{4} \quad (4.2a)$$

$$L2 + h = \frac{\lambda}{4} \quad (4.2b)$$

where λ is the wavelength of a signal at a certain frequency. In order to design the filter, the propagation velocity in the microstrip must be determined. This can be approximately determined using equation (4.3a) which is based on a curve-fit approximation [1] and using equation (4.3b)

$$\epsilon_e = \frac{\epsilon_r + 1}{2} + \frac{\epsilon_r - 1}{2} \frac{1}{\sqrt{1 + 12h/W}} \quad (4.3a)$$

$$v_p = \frac{c}{\sqrt{\epsilon_e}} \quad (4.3b)$$

where ϵ_r is the relative permittivity of the substrate of the microstrip, h and W are dimensions of the structure shown in Fig. 4.2, and c is the speed of light in free space. With these results, the filter can be designed for a specific frequency.

$$L1 = \frac{v_p}{4f_1} - h \quad (4.4a)$$

$$L2 = \frac{v_p}{4f_2} - h \quad (4.4b)$$

These equations are estimations, since the effective permittivity, ϵ_e , in microstrip is not the same for single-ended and differential and common modes. This is because in mixed-mode, a different proportion of the flux is in the dielectric as compared with single-ended.

4.3. Common Mode Filtering in Stripline Environments

Stripline architecture consists of two metal reference layers with the signal trace in between in the middle as in Fig. 4.3(a). The trace is surrounded by dielectric material. For differential transmission, the single trace is replaced with two coupled traces as in Fig. 4.3(b). This trace architecture is more convenient in multilayer boards and has less attenuation and radiation at higher frequencies as compared to microstrip.

Filtering using bowtie structures is accomplished in stripline much the same as in microstrip; a patch of metal with a via to reference. Just as with microstrip architecture, the filters consist of two quarter-wavelength resonators that are excited by common mode but not differential mode transmission. However, stripline traces couples very strongly with the reference planes which is broadside to the trace as compared with the edge-coupling to the other transmission line or to the filter. This results in limited filtering when no modification is made to the reference plane since the filter is not strongly excited. Voids in the ground plane can overcome this with limited effect to DM transmission.

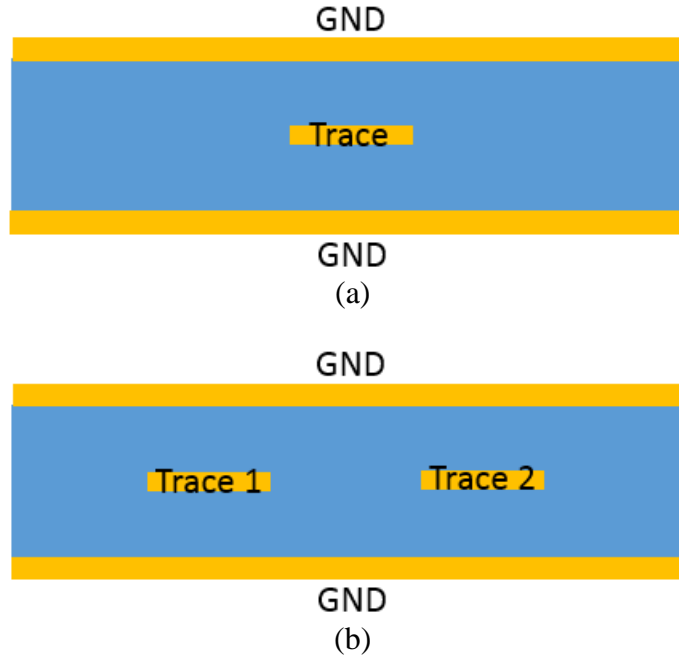


Fig. 4.3 - Stripline cross section in (a) single-ended and (b) mixed-mode configurations

Just as in microstrip, the filters attenuate most strongly when the length of the filter including the via distance to ground is a quarter of the wavelength. Unlike microstrip, the effective permittivity is equal to the permittivity of the dielectric material. This somewhat simplifies design because the predicted wavelength is not subject to inaccuracies of estimated formulas.

Voiding the reference planes as in Fig. 4.4 will result in a decrease in the coupling to the ground of the transmission lines. As the coupling to the reference planes decreases, a higher proportion of the flux couples to the filtering structure. This results in deeper filtering attenuation but may introduce a change in the differential impedance that hampers differential transmission. The size of the voids was chosen to be the same length as the filter with the width being as wide as the combined width of the transmission lines and the space between them. These dimensions did not significantly impact differential transmission.

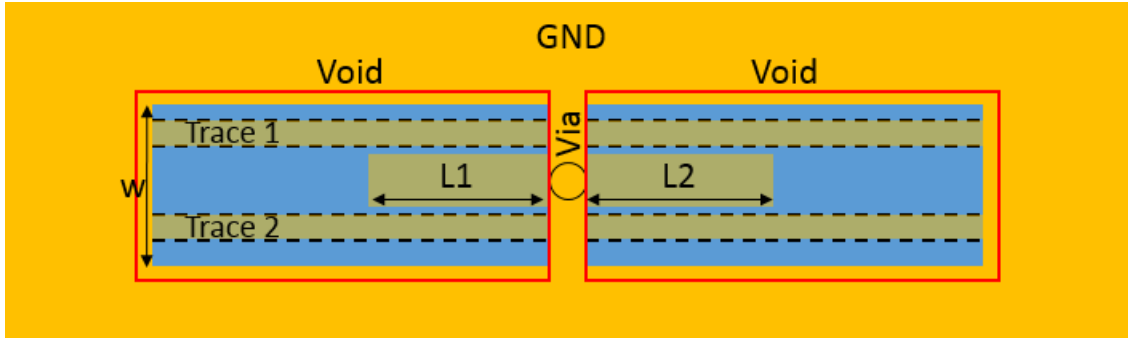


Fig. 4.4 - Differential stripline configuration with bowtie filter and voided ground planes

4.4. Common Mode Filtering in Broadside Coupled CPW

The Broadside Coupled CPW topology is especially good for common mode filtering due to the potential for strong coupling between the differential traces and a filtering element placed between the traces. The half wavelength bowtie structure can be implemented with great success in this structure. Additional filtering structures have been proposed and have shown promise, but they are not well characterized nor well understood.

In the case of a Broadside Coupled CPW, the bowtie structure is placed in a layer between the top and bottom differential traces. Instead of a via, shorting stubs are included near the center of the filter as in Fig. 4.5. The shorting pin connects from the filtering structure to a reference in the same plane or to vias that connect the top and bottom coplanar references. Another shorting pin is included on the opposite side of the filter to the other side of the reference or to the other via fence.

As in other architectures, the filter consists of two quarter wavelength resonators. The lengths $L1$ and $L2$ can be independently adjusted to achieve multiband filtering. Additionally, the distance from the filter to the reference, h , can be modified in this topology. This is in

contrast with stripline and microstrip where h is determined by the thickness of the substrate. Increasing this value allows for a shorter filter at a given frequency.

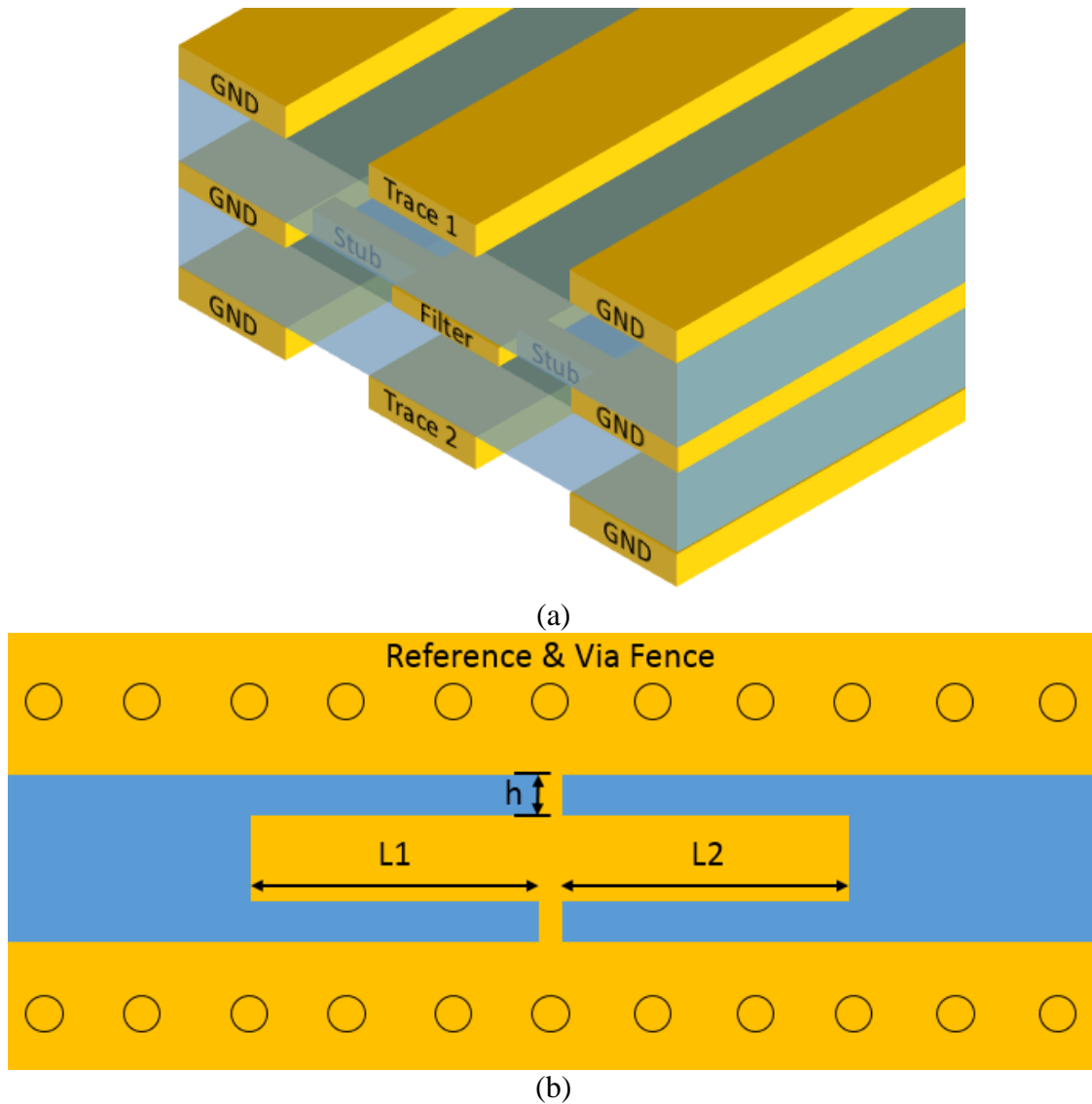


Fig. 4.5 - BC-CPW with a bowtie filter (a) perspective view and (b) top view of the filter layer

Because of the coupling strength of broadside coupling as compared with edge coupling, the filtering in this topology is both deeper and broader than in the analogous microstrip or stripline filter. The depth and breadth of filtering from a single filter in this topology suggests the use of only a single filter. A single structure can then be used to achieve effective, broadband filtering at multiple frequencies.

This topology is not yet well characterized, creating a slight difficulty in designing the filter. The propagation velocity and effective permittivity, in particular, have not been described by any design equations. At low frequencies, the single-ended effective permittivity is similar to but slightly lower than the effective permittivity of a microstrip with the same trace width and substrate thickness. At very high frequencies, the propagating mode is more confined within the dielectric, resulting in an effective permittivity that is close to the permittivity of the material. However, the propagating mode is not TEM at those frequencies; it is TE_{10} . This mode has both group and phase velocity which are not necessarily the same. The bowtie filter has only been examined at frequencies dominated by the TEM mode.

Due to these considerations, only an estimate about the filtering center frequency can be made. The bandwidth of the filter is large enough that an estimate suffices for most applications. When an estimate is inadequate, simulation can be used to analyze and predict the filtering frequency with a higher degree of confidence.

4.5. Differential Launch Structure for a Stripline Environment

The process for measuring a microstrip trace is rather simple. Connectors exist that can be bolted or soldered onto the edge of a test board and have very good transmission characteristics up to the frequencies at which microstrip begins radiating. In contrast, stripline requires a more sophisticated launch structure in order to be measured with RF probes or coaxial connectors. Specifically, a via transition is required from the top layer to the middle signal layer. Since the signal trace is in the middle, a stub will be left below the trace (as in Fig. 4.6) due to back drilling in the manufacturing process.

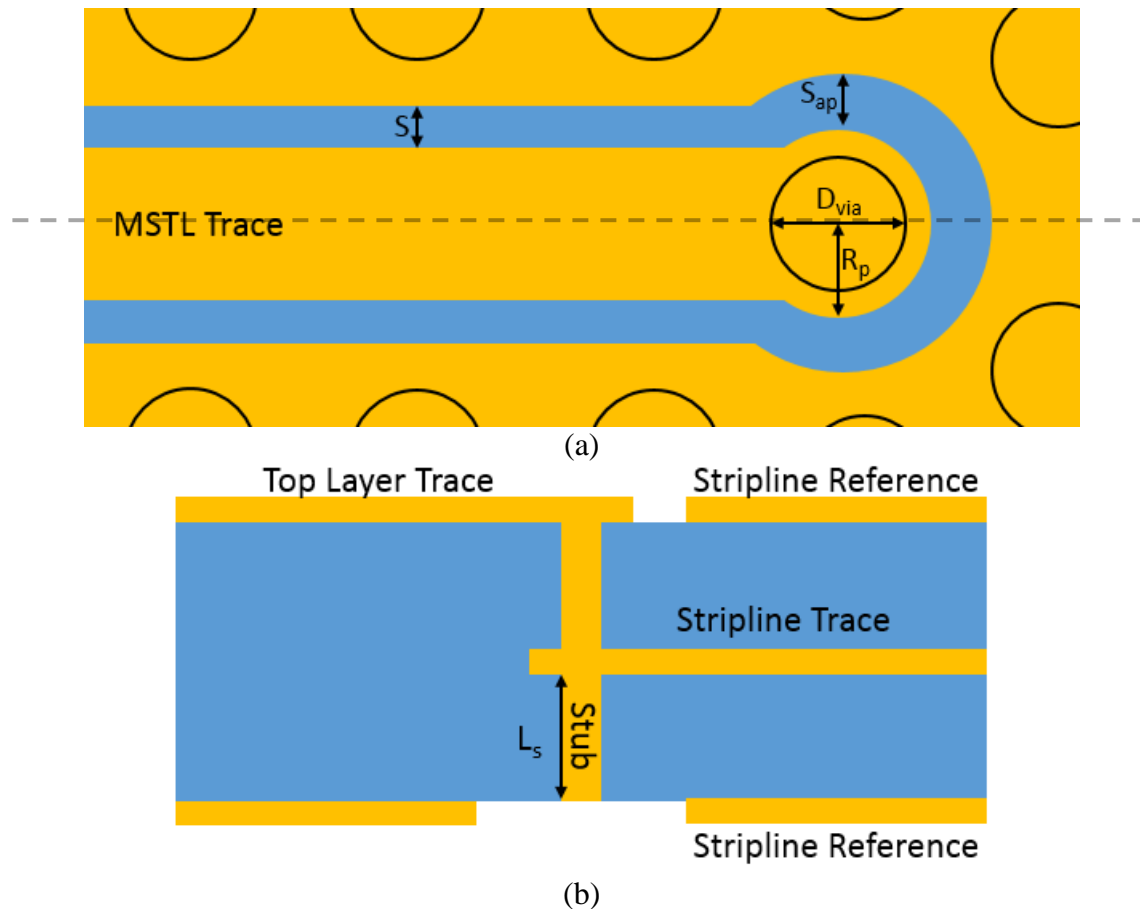


Fig. 4.6 - Stripline transition (a) top view and (b) cross-section cut at the dotted line showing via and stub

The requirement for this transition poses several signal integrity and EMC challenges. First, the via is a discontinuity that results in an impedance change and thus reflections. The stub has a resonance associated that, when excited, will act as a filter, preventing transmission. The via also has the potential to excite parallel plate waveguide modes, which, in addition to radiating energy and harming transmission, can couple to the other differential trace and cause mode conversion. If a parallel plate mode is excited, energy can be unintentionally transmitted and interfere with circuitry in other areas of the printed circuit board.

The first challenge to be overcome is matching the transition to the launch. A coplanar waveguide is used as a launch pad for the transmission line that runs from the input to the via transition. The coplanar waveguide is designed to be 50 ohms. The transition should thus also

be designed to be 50 ohms. A pad must be included for the via. This pad will be slightly wider than the coplanar waveguide trace, resulting in slightly increased capacitance. As a result, the antipad must leave a gap to the reference that is slightly larger than the gap in the coplanar trace. The via itself has capacitive coupling with the upper reference plane. The via is naturally inductive, so the impedance will be approximately correct. Since the transition is relatively small, the impedance must only approximately match the coplanar and stripline impedances. The closer the match is, the higher in frequency the transmission will survive. Ultimately, a physics-based design followed by simulation and modifications suffices for most applications.

The stub can be modeled as a transmission line terminated by a capacitance. If the stub were open circuited, a resonance would exist at the frequency where $L_s = \frac{\lambda}{4}$. Since the stub is instead terminated in a capacitance, the resonance is shifted. The impedance at the trace side of the stub looking toward the open circuited end is

$$Z_{in} = Z_c \frac{Z_L + jZ_c \tan \beta l}{Z_c + jZ_L \tan \beta l} \quad (4.5a)$$

$$\text{At resonance:} \quad Z_L = -jZ_c \tan \beta l \quad (4.5b)$$

If the transmission line were purely open circuited,

$$\text{At resonance:} \quad O.C. = -jZ_c \tan \beta l \quad (4.6)$$

The capacitance serves to shift the resonance down in frequency. The larger the capacitance is, the lower the resonant frequency will be. Clearly, this capacitance should be minimized. This can be accomplished by making the void around the end of the stub large. However, if the void is too large, it will have an effect on the impedance of the stripline, since it will alter the capacitance from the signal trace to the reference. This effect is small, so the void can be made large enough to negate the effect of the capacitance.

Parallel plate waveguide mode excitation is avoided through the use of via fencing around the launch structure. The via fencing serves to isolate the launch structure from other areas on the PCB. Additionally, several vias are used to prevent coupling between the signal via transitions.

4.6. Differential Launch Structure for Broadside Coupled Coplanar Waveguide

Like the stripline topology, the BC-CPW topology requires a launch that includes a via transition in order to be measured. However, the BC-CPW has the added difficulty of requiring an asymmetric launch to be probed from a single side. Asymmetry can result in common mode conversion, and since the primary purpose of this topology is compact and strong common mode filtering structures, common mode conversion must be firmly avoided. The launch structure must be carefully designed than, so as to mitigate common mode conversion to the greatest extent possible. This can be accomplished through a combination of impedance matching to prevent asymmetric reflections and length compensation to mitigate skew.

A via transition is only needed in one of the two differential traces since only one of the traces will be on the opposite side of the board from the input. On both traces, an MSTL runs from the input. In the first trace, the MSTL continues into the device under test. In the second trace, the MSTL goes to a via that goes through the board into another MSTL on the other side. Two primary challenges exist in creating this launch structure. The via transition must be matched to allow for good transmission on that trace and to avoid common mode conversion that comes from mismatch between the two traces. Secondly, the difference in length that comes from one trace having to run through the board and the other going directly to the device under test must be accounted for and compensated.

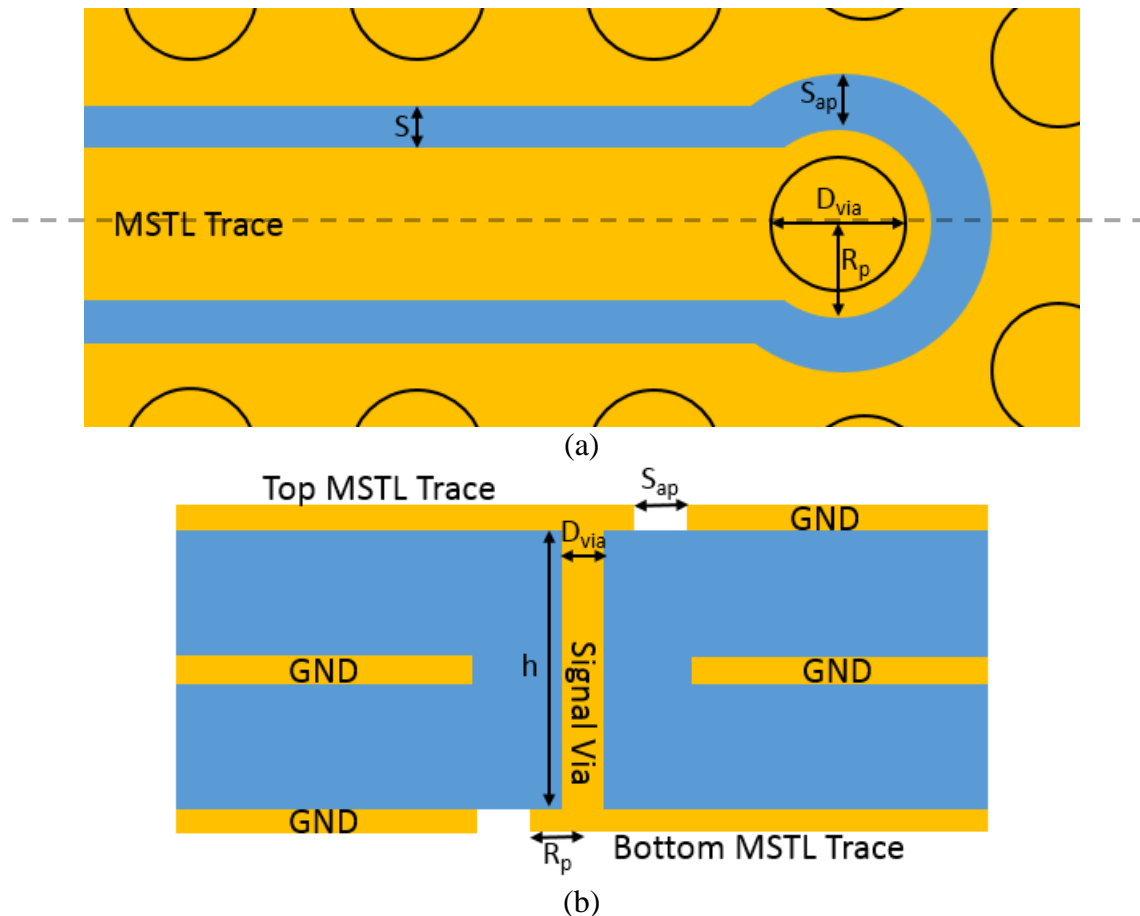


Fig. 4.7 - BC-CPW launch transition (a) top view and (b) cross section cut at the dotted line

The via transition consists of a pad on both the top and bottom metal layers, an antipad on each of these layers, and the via. The pad is wider than the MSTL trace, so it will raise the capacitance of the trace. To compensate for the pad, the antipad gap, S_{ap} , is made wider than the gap between the MSTL trace and reference. The via diameter, D_{via} , is roughly fixed by the process parameters and cannot be finely adjusted. As with the stripline, for most frequencies of interest the transition is relatively small electrically, however, the BC-CPW is intended for higher frequency operation than stripline so more care must be taken in the design. Additionally, mismatch in the stripline launch resulted in degraded transmission. Mismatch in the BC-CPW launch results in common mode conversion which should certainly be avoided. The same cycle

of a physics-based design followed by simulation and modification is taken in this structure, but with more iterations to arrive at a better match.

The length is compensated for in the MSTL section of the launch. The trace without the via transition is compensated with a length equal to the effective length of the via transition. The first approximation of this length is just the height of the board without the outer metal layers, h . Since the propagation velocity is not the same in the via transition as it in the MSTL, this will not compensate exactly, but it will be close enough to serve as a start. After simulation, modifications can be made to this length to compensate for the path length difference more closely.

5. FILTER AND LAUNCH STRUCTURE DESIGN AND VALIDATION

The microstrip, stripline, and BC-CPW filter models and the stripline and BC-CPW launch models are validated through computer simulation and measurement of fabricated structures. A minimum of three filtering structures were simulated and fabricated for each topology of microstrip, stripline, and BC-CPW. RF probe signal launches were simulated and fabricated for both stripline and BC-CPW topologies. Additionally, a coaxial signal launch structure was simulated, fabricated, and measured for the BC-CPW topology. These signal launches were used in measuring the filtering structures in stripline and BC-CPW. The computer model and fabricated version of the test board with the BC-CPW and stripline structures are shown in Appendix B.

In order to have maximum confidence in the performance of the structures proposed, each is both simulated and measured. The simulation results and the measurement are compared to ensure the simulation reflects reality as closely as possible. The comparison of these results serves to confirm the accuracy of the simulation. Once the simulations are matched to physical measurement, additional simulations can be undertaken with an added degree of trust that these simulation results might be replicated in a physical structure.

For the filtering structures, the primary characteristics examined are the frequencies of operation and the attenuation. In comparison with the theoretical model, the center filtering frequency should match within a certain margin of error that depends upon the topology and the assumptions made. The impact of the filters on the differential mode transmission is predicted to be negligible. Any major impact on the differential mode transmission caused by the filtering structures represents a deviation from the theoretical predictions. When comparing simulated and measured results, the band of the filter is primarily considered. This includes the frequencies

of the edges of the stopbands, the frequency of strongest filtering, and the overall attenuation. Overall, the simulated and measured results should match closely, but some tolerance is given to allow for manufacturing tolerances, dielectric mismatch, and other attributes not considered by the simulation.

Both frequency and time domain analysis, simulation, and measurement are employed in this investigation. We use mixed-mode scattering parameters (frequency-domain) and the impedance as inferred through time domain reflectometry (TDR). Scattering parameters are discussed in section 2.4, but in short, they characterize the effect the device measured has on signals at different frequencies. The specific scattering parameters examined for validation are S_{dd21} , which is effectively the transmission from port 1 to port 2 in differential mode, S_{cc21} , which is effectively the transmission in common mode, and S_{cd21} , which is effectively the conversion of differential mode signal to common mode signal from port 1 to port 2. TDR is a time domain based experimental probe which characterizes system characteristics based on the reflections from an excitation in the form of a short pulse in the time domain (17 ps rise time). From these reflections, the relative impedance can be mapped as a function of distance traveled. This TDR measurement can be used to examine the characteristic impedance at various points in the structure and check for mismatch, which is particularly useful in the revisions of the launch structure for matching the transitions to the traces.

The measurement setup used for all devices is shown in Fig. 5.1. In the figure, the measurements being taken are single-ended scattering parameters at port 1 and port 4 of the DUT with the other ports terminated in matched loads. From equations 2.21(a-d), the single-ended scattering parameters S_{11} , S_{13} , S_{31} , S_{33} , S_{21} , S_{41} , S_{23} , and S_{43} must be taken. In real passive devices, the scattering parameter matrix is symmetric, so only S_{31} or S_{13} must be taken since

they are equal. To obtain these single-ended scattering parameters, five configurations are needed. These configurations will be denoted as follows: the DUT port to which VNA port 1 is connected-the DUT port to which VNA port 2 is connected. Any DUT port not connected to the VNA is terminated in a matched load. For example, the configuration in Fig. 5.1 is denoted 1-4. To obtain the eight necessary single-ended scattering parameters, the following configurations are needed: 1-2, 1-3, 1-4, 3-2, 3-4. Once the single-ended scattering parameters are obtained, they are converted to mixed-mode scattering parameters using equations 2.21(a-d).

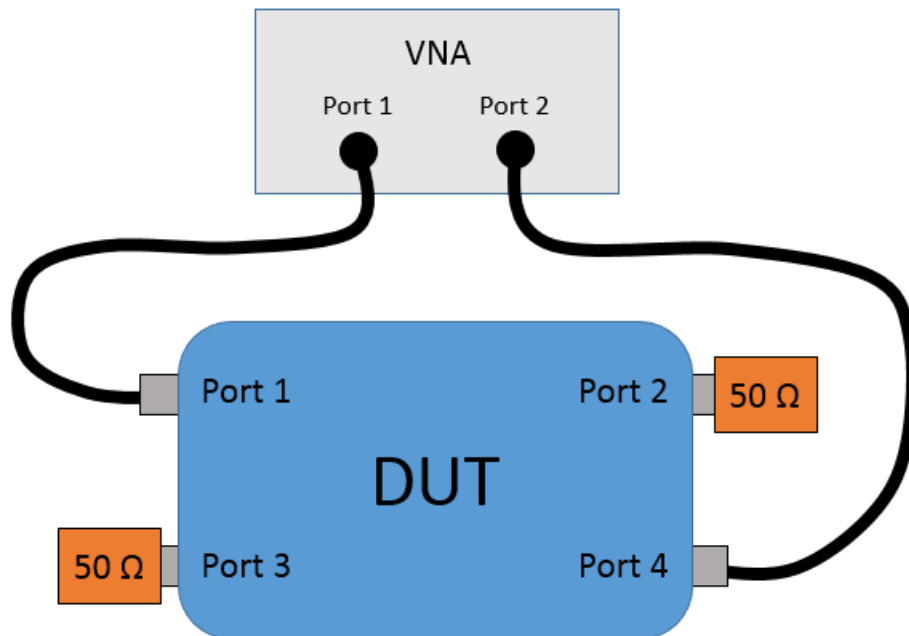


Fig. 5.1 - Setup used to measure mixed-mode scattering parameters

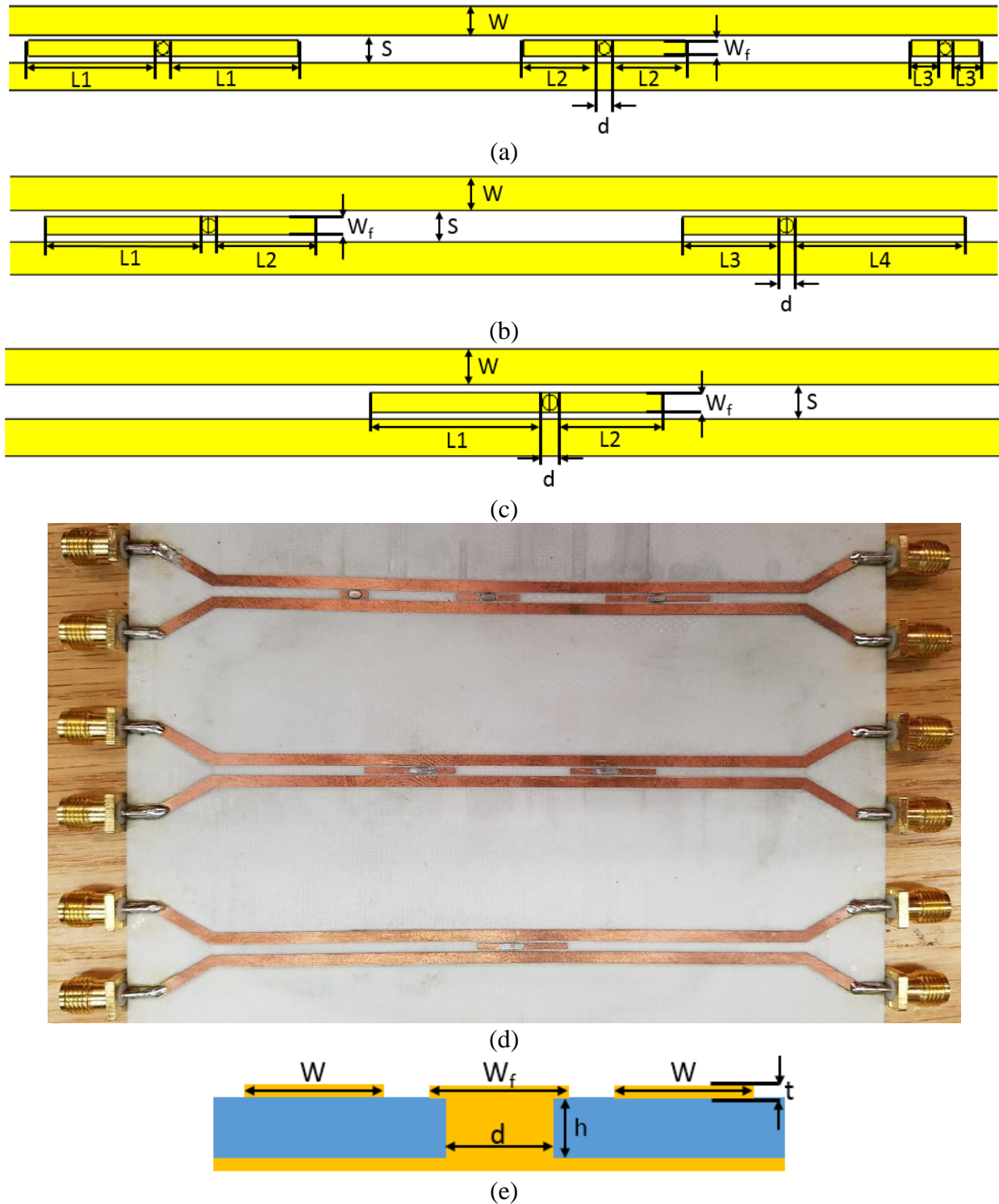
5.1. Microstrip Filtering Structures

Fig. 5.2 - (a-c) Top view of all three filtering structures for microstrip lines, (d) the fabricated structures and (e) the cross section

Table 5.1

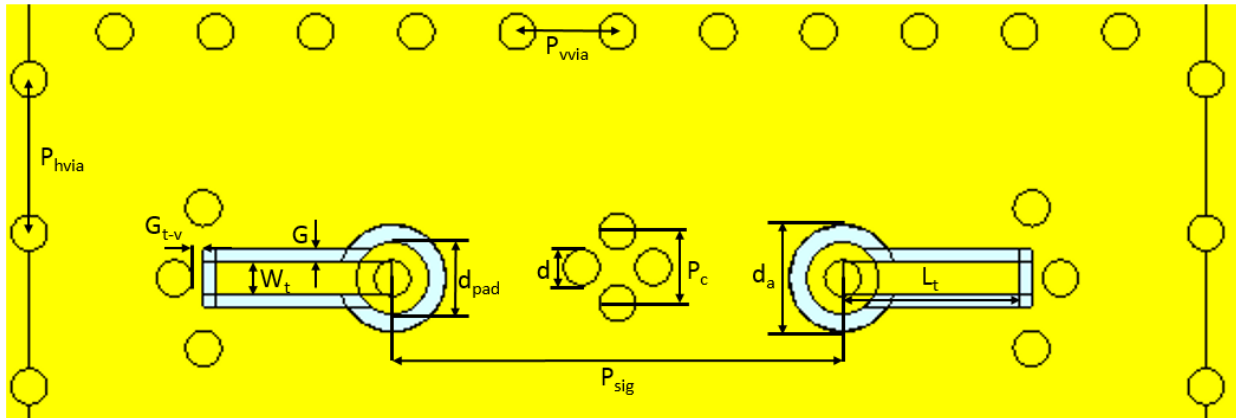
Structure	Dimensions (mm)		Material Properties
	W	1.88	$\epsilon_r = 3.0$
	S	1.88	$\epsilon_e = 2.41$
	W_f	1.00	
	T	0.035	Material: Rogers 4730
	h	0.77	
	d	0.8	
			Predicted Filter Frequency (GHz)
(a)	L1	8.6	5.15
	L2	5.0	8.37
	L3	1.9	18.08
(b)	L1	8.6	5.15
	L2	5.5	7.70
	L3	5.31	7.94
	L4	9.35	4.77
(c)	L1	9.06	4.91
	L2	5.47	7.74

Three filtering structures were simulated, fabricated, and measured in the microstrip topology. The first filtering structure consists of three bowtie filters each with a centered via targeted at a different frequency. The second structure consists of two bowtie filters with shifted vias targeted at the same two frequencies. The third structure consists of a single bowtie filter targeted at two frequencies through the use of a shifted via. These designs are shown in Fig. 5.2 and the dimensions are given in Table 5.1.

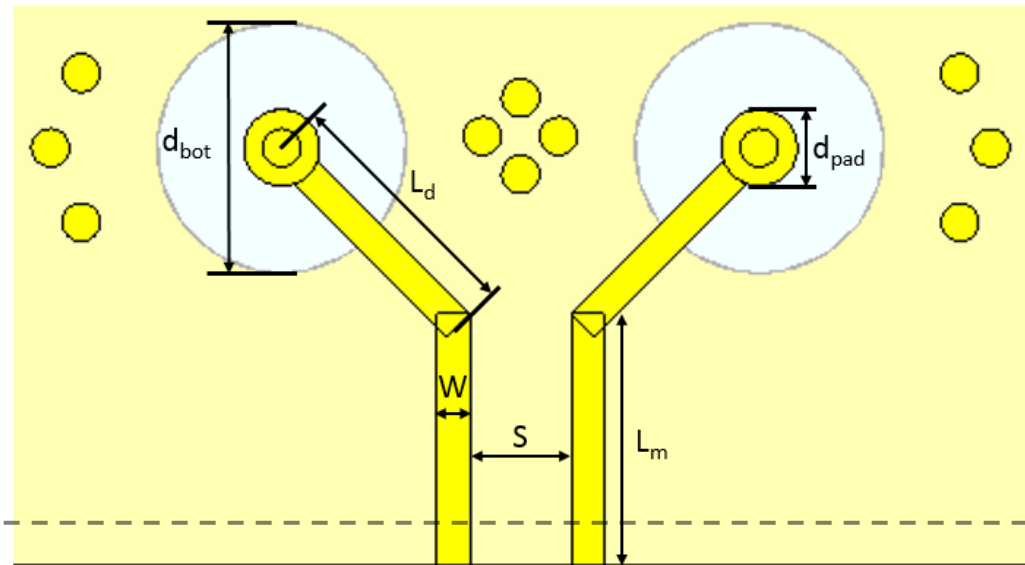
5.2. Stripline Launch Structures and Filters

The RF probe signal launch structure is designed to operate from 0 - 20 GHz. The goal is to have S_{dd21} be greater than -1 dB, that is no more than 1 dB of differential mode insertion loss, over the operating range. The DUT had predetermined dimensions that the launch structure had to match at the end. To this end, the structure was designed as in Fig. 5.3 with the dimensions

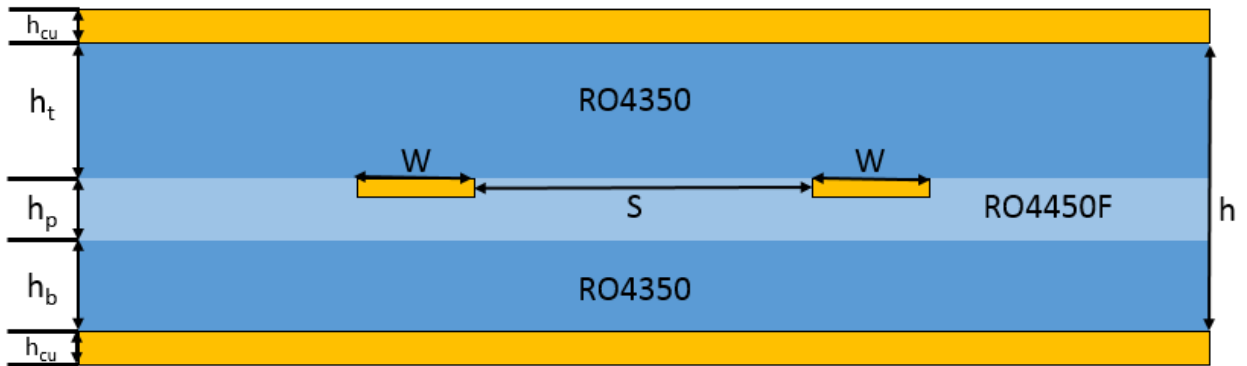
listed in Table 5.2. Additionally, a set of TRL calibration standards were fabricated to enable de-embedding of the launch structure and to allow isolating the effects of the filtering structures.



(a)



(b)



(c)

Fig. 5.3 - (a,b) Top view of the (a) top layer and (b) middle layer. (c) Cross section at the dashed line in (b)

Table 5.2

Dimensions (mm)				Material	Relative Permittivity
d	0.3048	L_d	3.0	RO4350	3.66
d_a	0.9144	L_m	3.0	RO4450F	3.52
d_{bot}	2.0	L_t	2.0		
d_{pad}	0.6096	P_c	0.6096		
G	0.106	P_{hvia}	1.3048		
G_{t-v}	0.094	P_{sig}	3.826489		
h	0.55372	P_{vvia}	0.8548		
h_b	0.16764	S	0.8128		
h_{cu}	0.035	W	0.262		
h_p	0.1143	W_t	0.274		
h_t	0.254				

Four stripline-based filtering structures were simulated and fabricated. The first three structures, structures (**a1-3**), consist of a single bowtie filter with a centered via each at a different frequency of filtering. The last structure consists of a cascade of three bowtie filters, each designed to filter at the frequencies from the first three single bowtie filters. This cascade structure is used to investigate the feasibility of cascading filters in one like in order to filter at multiple frequencies. The single filter design is shown in Fig. 5.4a and the multi-filter design is shown in Fig. 5.4b. The dimensions are given in Table 5.3. The cross section of the transmission lines remains the same as the cross section at the end of the launch structure.

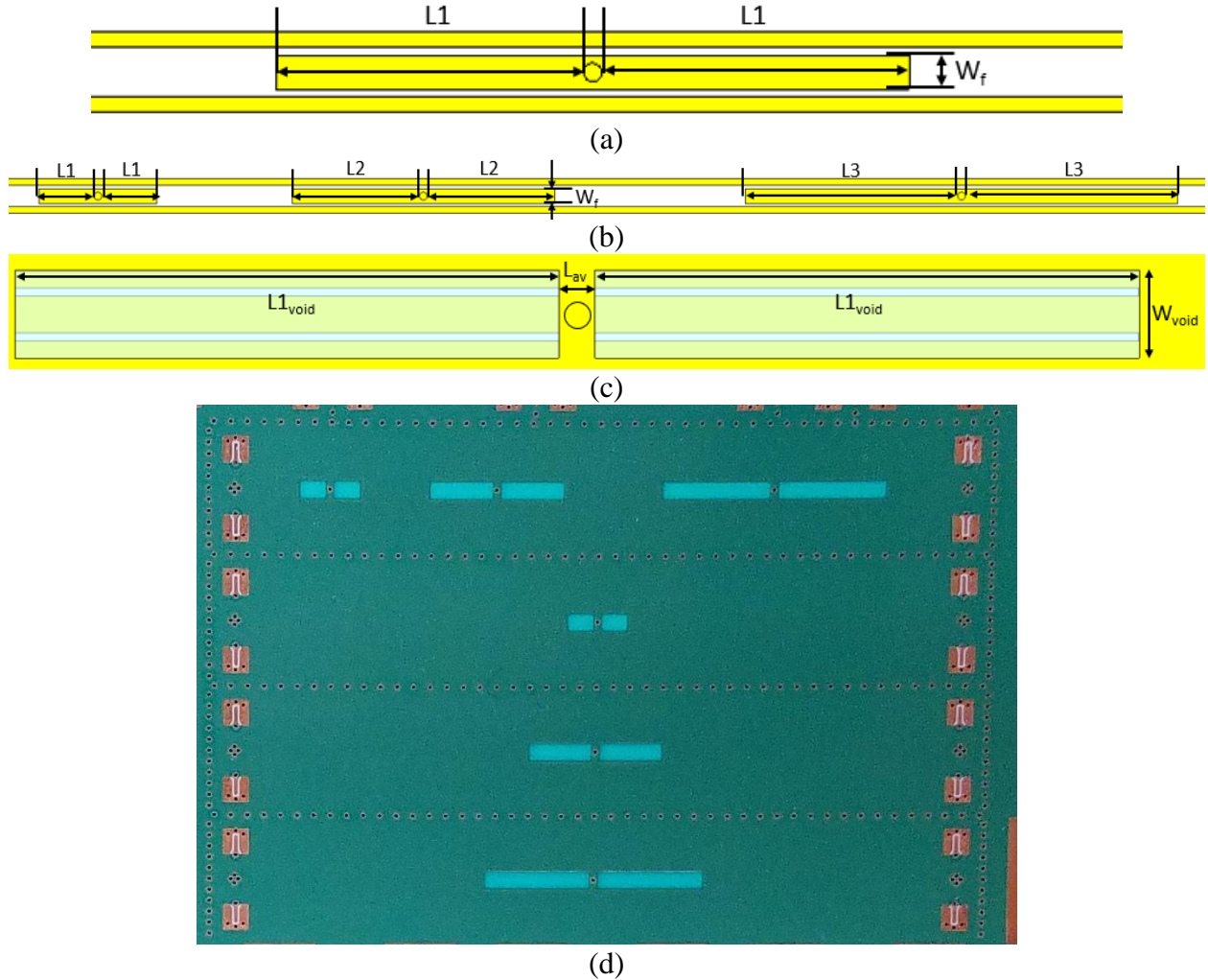


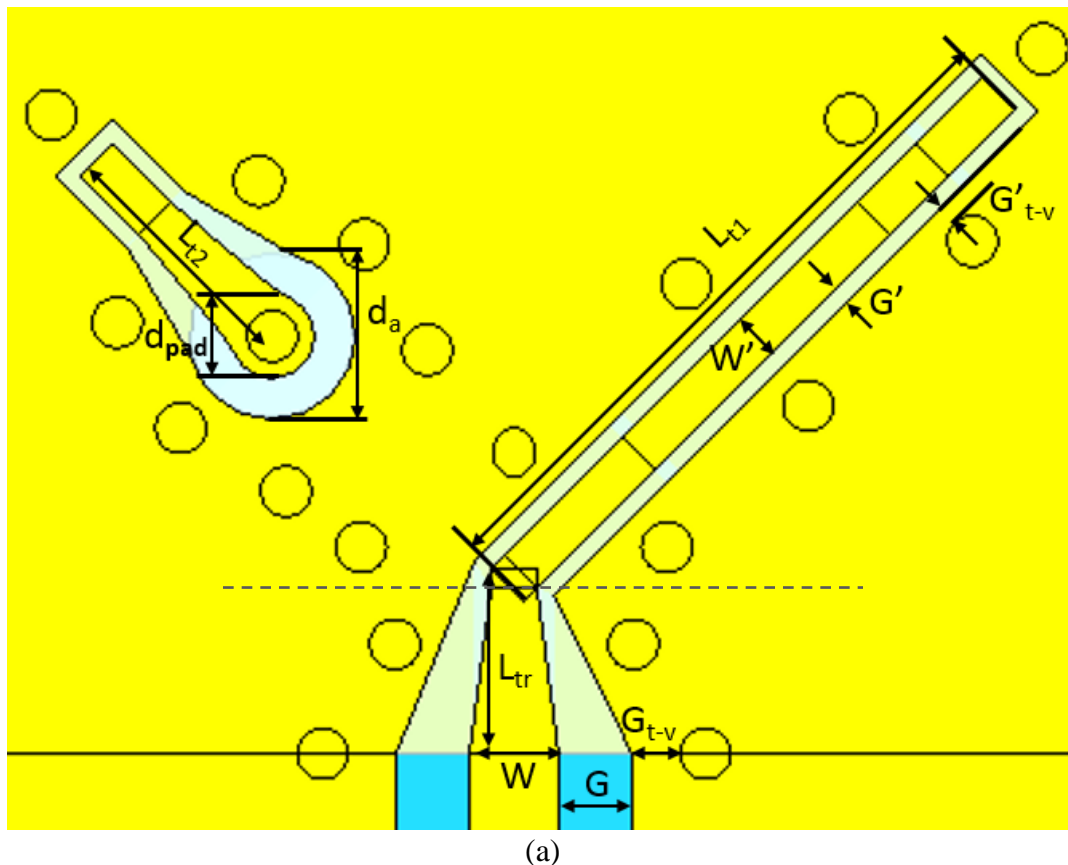
Fig. 5.4 - Top view of (a,b) the middle layer of stripline filter structures, (c) the top view of the structures showing the void in the top and bottom reference planes, and (d) the fabricated structures

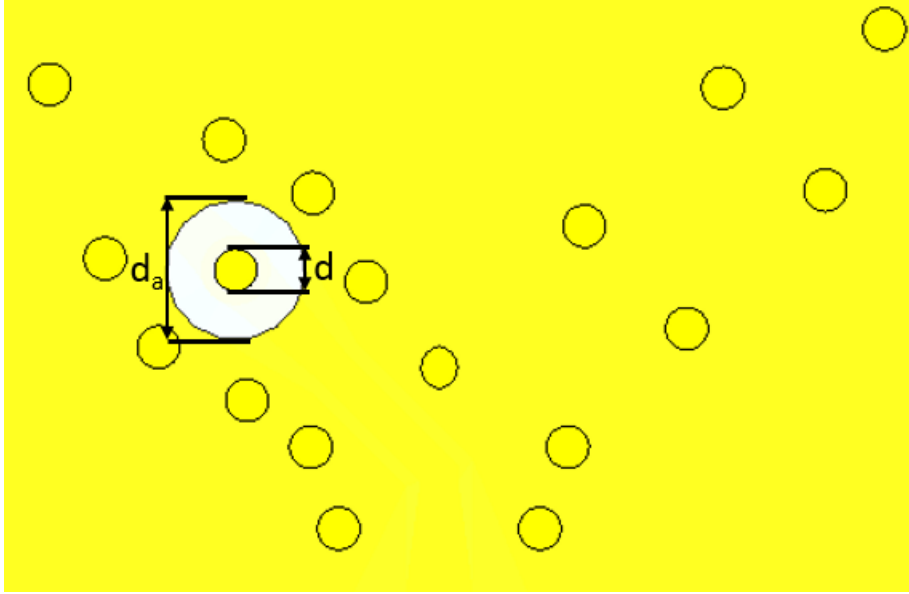
Table 5.3

Structure	Dimensions (mm)				Predicted Filter Frequency (GHz)
(a1)	W_f	0.5588			17.34
	L_{av}	0.5588			
	W_{void}	1.3368			
(b)	L1	2.2026	L1 _{void}	2.0756	15.80
	L2	5.0876	L2 _{void}	4.9606	7.58
	L3	8.4976	L3 _{void}	8.3706	4.60

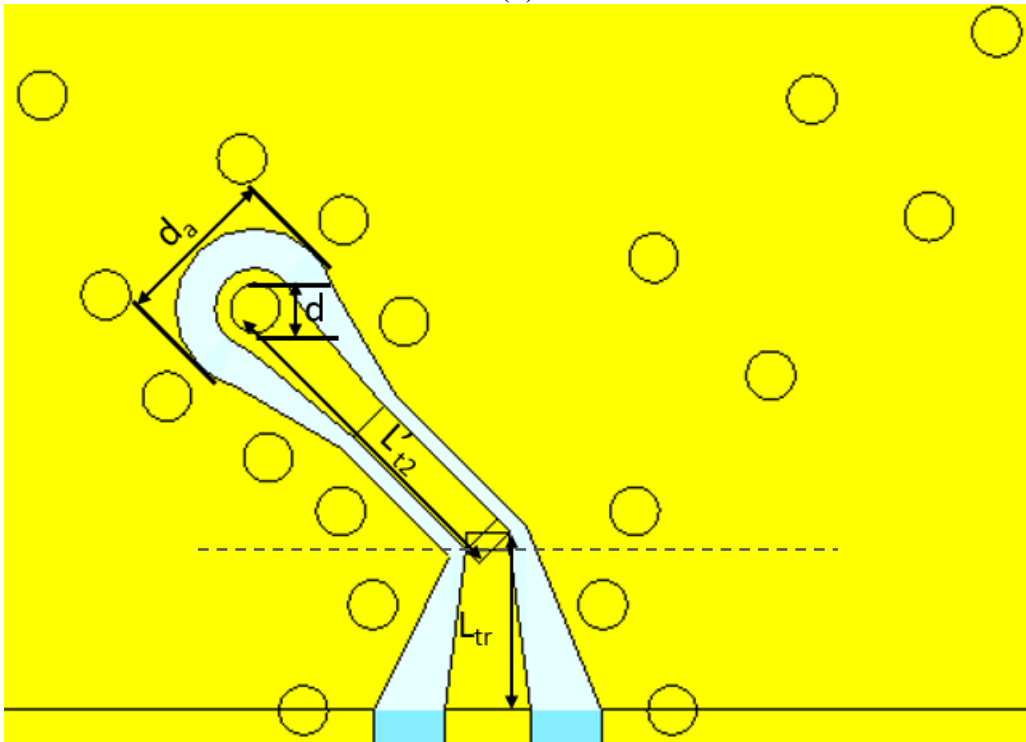
5.3. Broadside Coupled Coplanar Waveguide Launch Structure and Filters

Two types of launch structures were designed to operate from 0-40 GHz for the BC-CPW topology. The first type is for the RF probing station and the second is for a coaxial connector. The via transitions were nearly the same between the two types with the top trace needing to be rotated slightly in order to make room for coaxial connectors which are larger than the RF probes. The via transitions were nearly the same between the two types with the top trace needing to be rotated slightly in order to make room for coaxial connectors which are larger than the RF probes. These launch structures were designed to have S_{cd21} less than -20 dB and S_{dd21} greater than -3 dB from 0 to 40 GHz. The MSTL traces were designed for 50 ohms, since both the RF probe and the coaxial connectors are 50 ohms. The DUT have predetermined dimensions and are not 50 ohms, requiring a taper from the 50 ohm MSTL trace to the DUT BC-CPW trace which compromises S_{dd21} . The launch structures and DUT BC-CPW trace cross section are shown in Fig. 5.5, and the dimensions are given in Table 5.4.

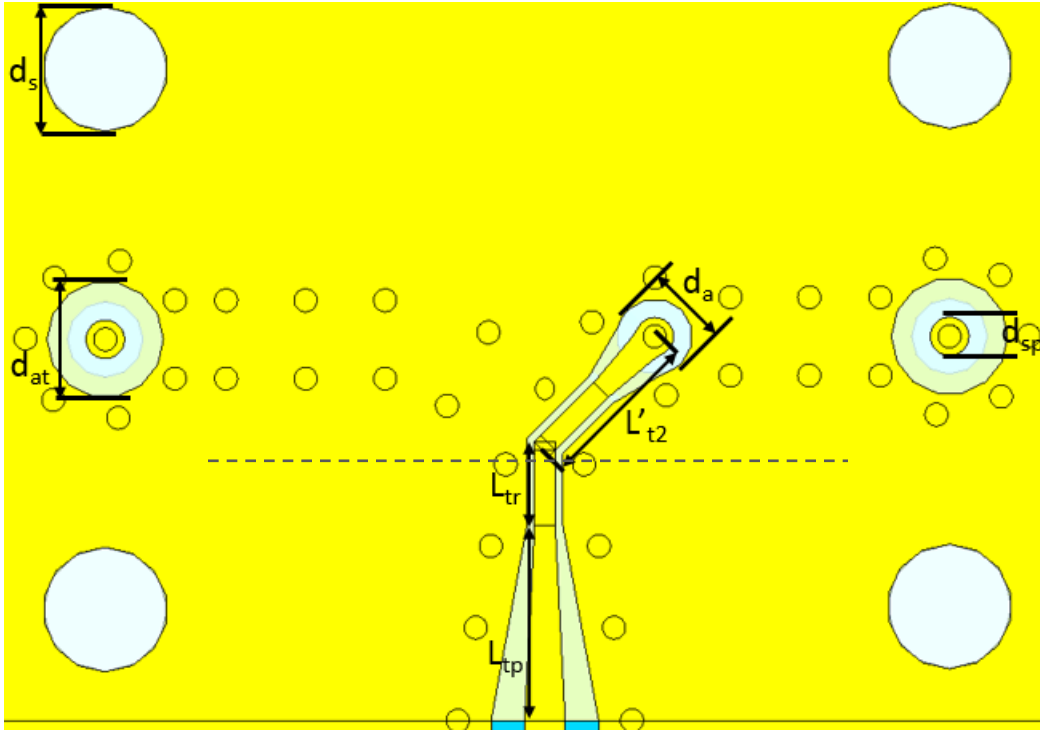




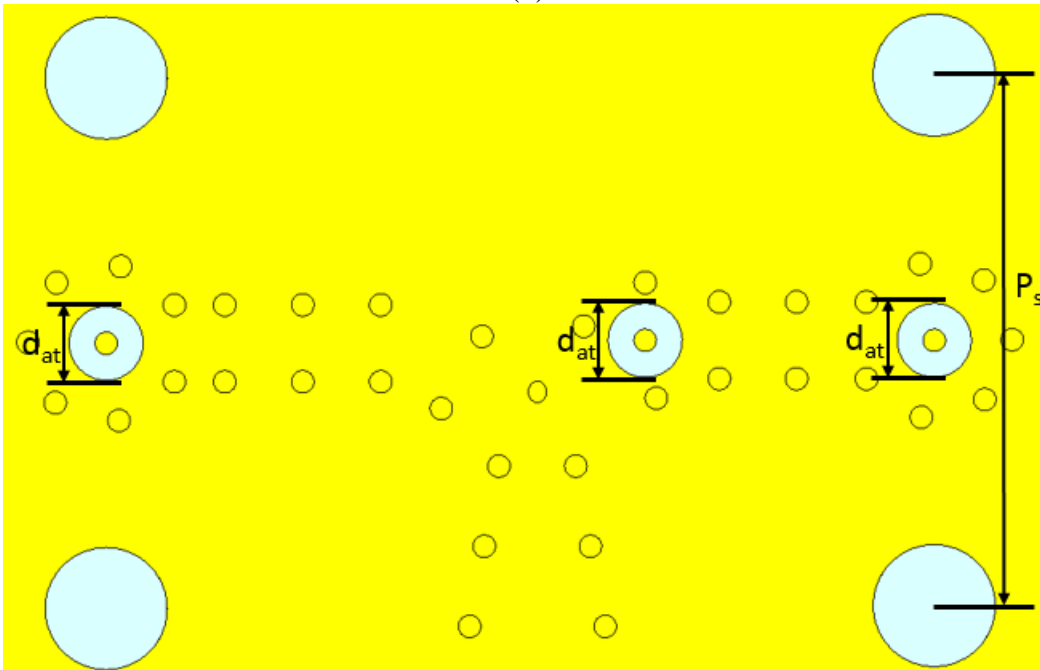
(b)



(c)



(d)



(e)

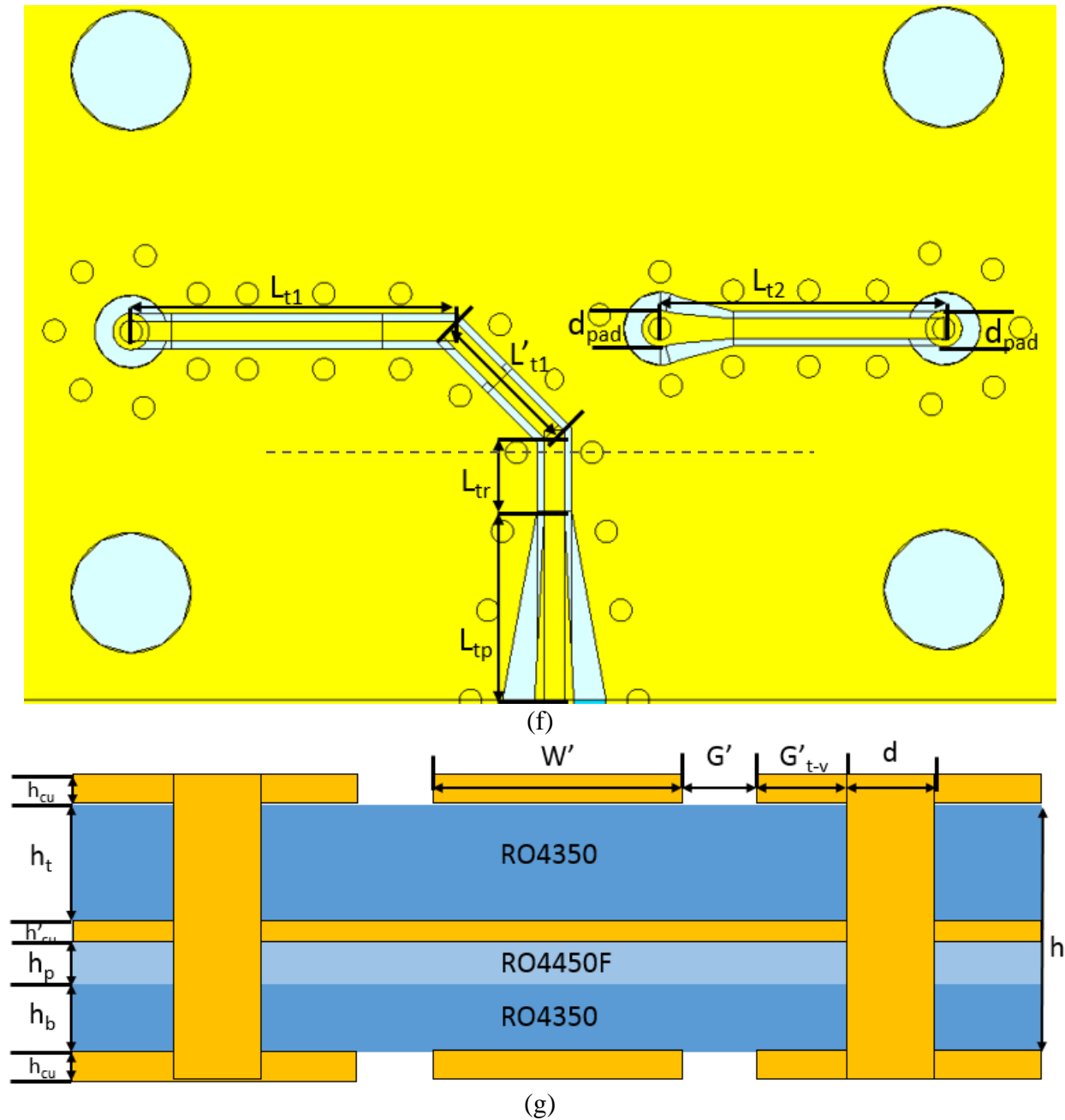
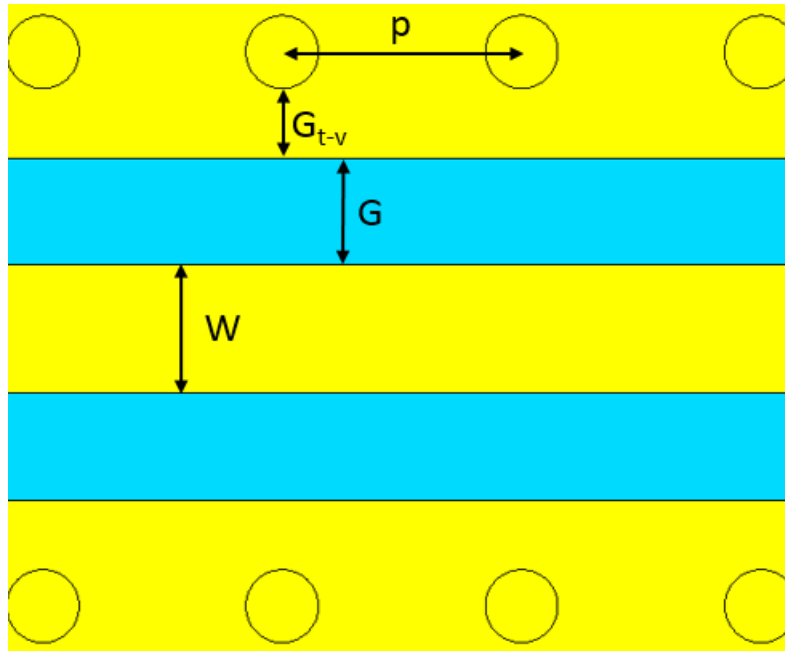


Fig. 5.5 - Top views of the RF probe signal launch structure (a) top layer, (b) middle layer, and (c) bottom layer and the top views of the coaxial signal launch (d) top layer, (e) middle layer, and (f) bottom layer. (g) Cross section of the 50 ohm BC-CPW used before the taper (shown as a dotted line)

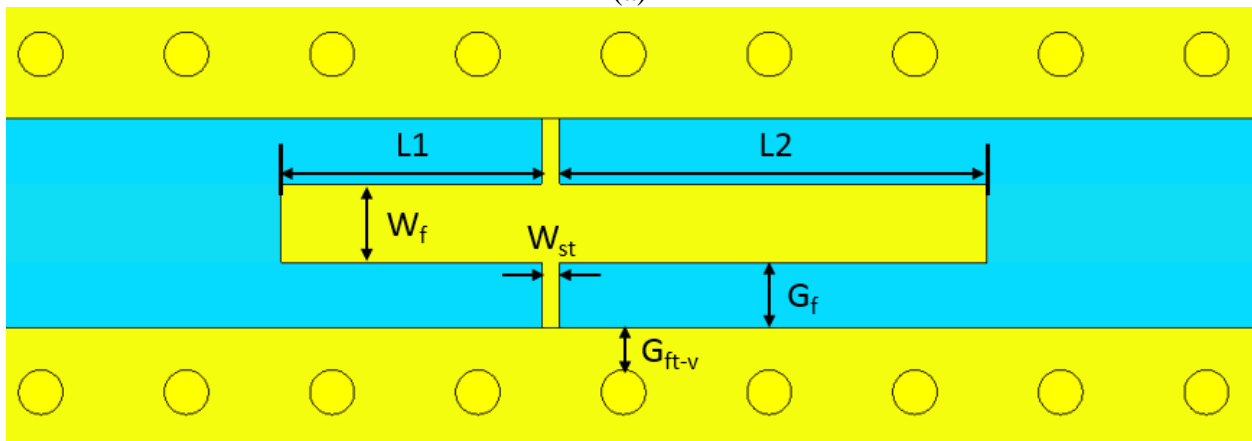
Table 5.4

Common Dimensions Between Coax and RF Probe Launch (mm)		Dimension Differing Between Coax and Probe Launch (mm)		
			Coaxial Launch	Probe Launch
W	0.536			
G	0.4432			
G_{t-v}	0.2888			
W'	0.274			
G'_{t-v}	0.1272			
G'	0.1017			
d	0.3048			
d_{pad}	0.5	d_{sp}	0.51	N/A
d_a	1	d_{at}	1.54	N/A
h_{cu}	0.04318	d_s	1.65	N/A
h_t	0.254	P_s	7.16	N/A
h'_{cu}	0.01778	L_{t1}	4.46	4.173
h_p	0.096266	L'_{t1}	2.113	N/A
h_b	0.16764	L_{t2}	3.9	1.5
h	0.535686	L'_{t2}	2.113	2.113
L_{tr}	1.113	L_{tp}	2.58	N/A

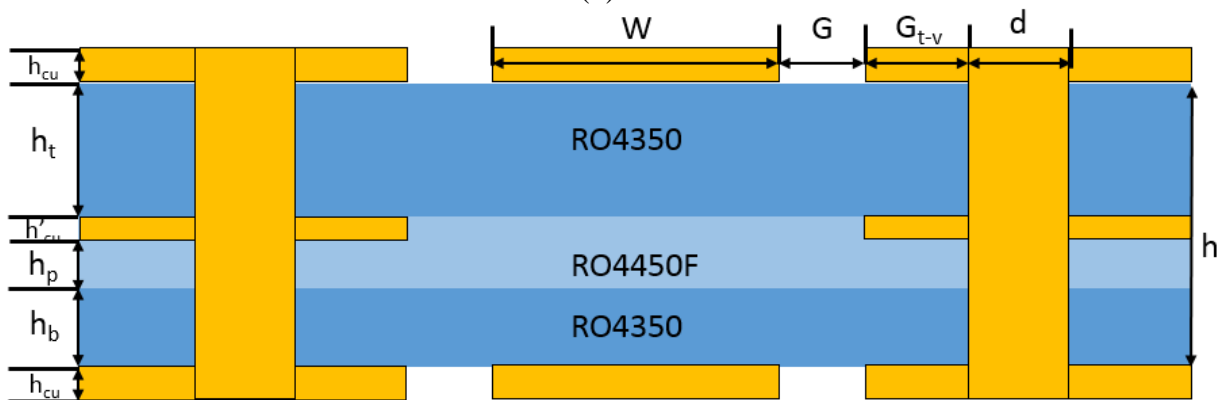
In total, six filtering structures were simulated, fabricated, and measured. The first three structures each have a single filtering element, structures **(a-c)** respectively. The next filter has a cascade of filters **(a-c)**. The second to last structure is **(b)** and **(c)** cascaded. The final structure consists of just filter **(d)**. Each of the six filtering structures was simulated, fabricated, and measured with the coaxial signal launch. In addition, the final three structures were fabricated with the RF probe signal launch. Two transmission lines of different lengths that have no filtering structures were fabricated with both the RF probe signal launch and the coaxial signal launch. The structures are shown in Fig. 5.6. The dimensions specific to the filtering layer are given in Table 5.5.



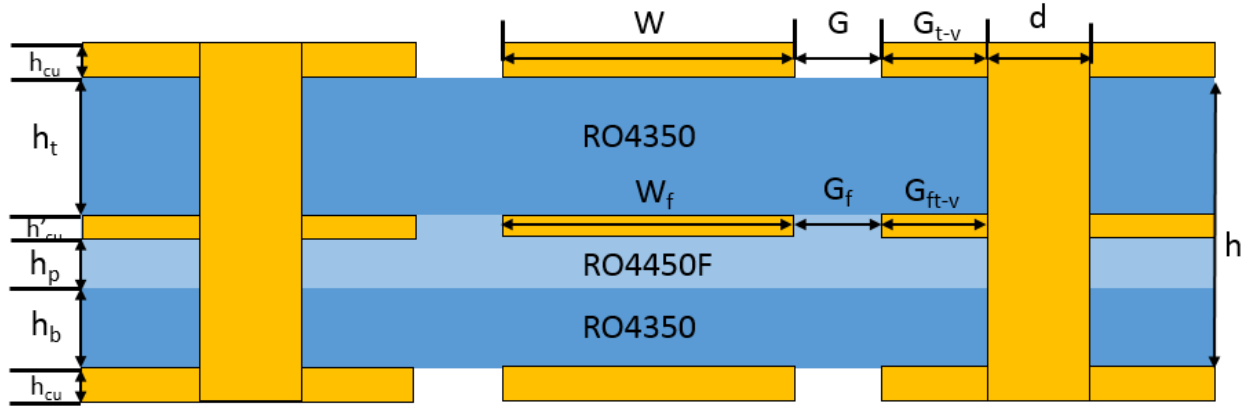
(a)



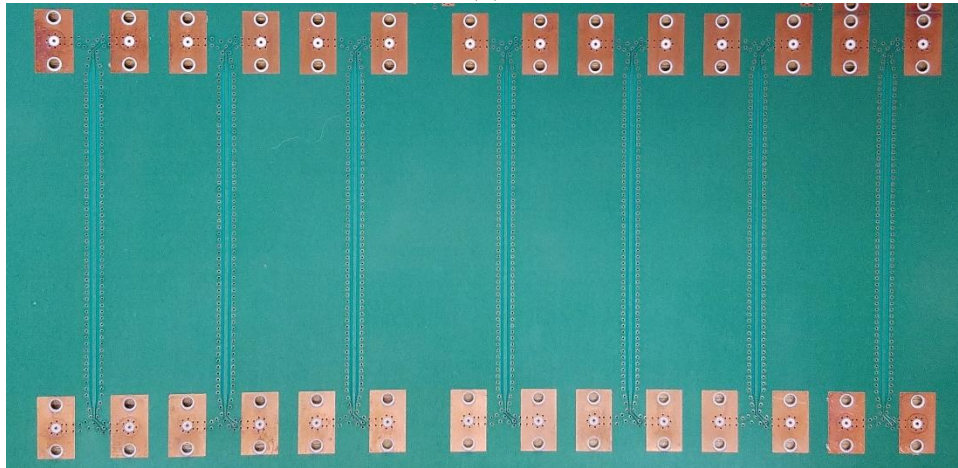
(b)



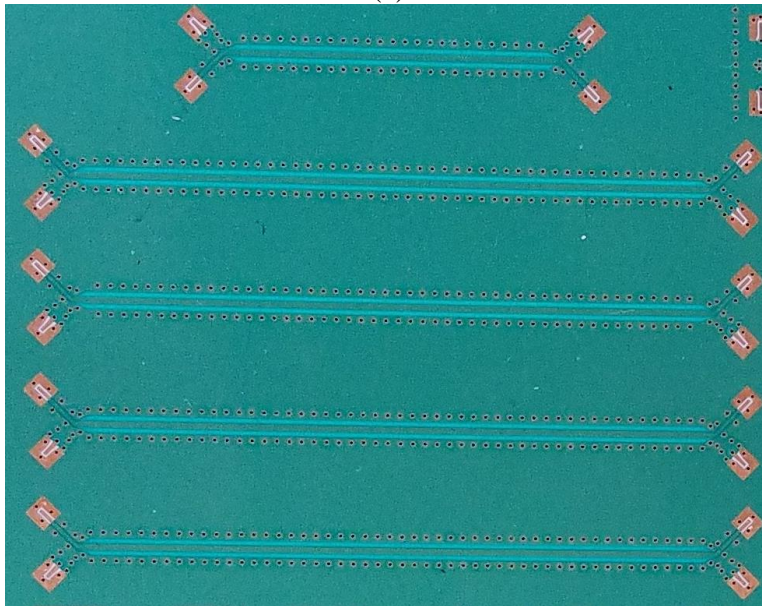
(c)



(d)



(e)



(f)

Fig. 5.6 - Top views of the (a) trace and (b) filtering structure. Cross sections of (c) the trace without a filtering structure and (d) with a filtering structure. Pictures the fabricated devices (e) with the coaxial launch structures and (f) with the RF probe launch structures

Table 5.5

Dimensions (mm)			
	W_f	0.536	
	W_{st}	0.125	
	G_f	0.4432	
	G_{ft-v}	0.2888	
Filter			Predicted Filter Frequency (GHz)
(a)	L1	4.31	8.13
	L2	4.31	8.13
(b)	L1	2.934	11.4
	L2	2.934	11.4
(c)	L1	1.787	17.1
	L2	1.787	17.1
(d)	L1	2.934	11.4
	L2	1.787	17.1

6. PERFORMANCE AND DISCUSSION OF LAUNCH STRUCTURES AND FILTERS

For the launch structures, measured and simulated S_{dd21} and S_{cd21} are plotted over the frequency range of operation, with lines denoting the goal for S_{dd21} . TDRs are also plotted for certain launch structures to show the impedance changes in the launch structures.

For each filtering structure, measured and simulated S_{dd21} and S_{cc21} are plotted against frequency. A vertical line is plotted at the design frequency in order to allow a quick visual comparison of the design frequency and the actual filtering frequencies.

From the plots, it can be seen that the simulated and measured results match fairly well in most cases. In most cases, small discrepancies existed between simulated and measured primarily in the frequencies where characteristics exist. However, more significant differences between simulation and measurement are present in some of the structures. These differences could be due to any number of factors, and additional work must be done to determine the causes of these differences. Some possibilities are discussed in the below.

In the filtering structures, predicted filtering frequencies give estimates of the center frequencies of the filtering structures but cannot be relied on for accurate predictions. Therefore simulation should be done to ensure that the stopband frequency range is acceptable. The filtering attenuates common mode signal more by more than 10 dB in all filtering structures and attenuates by up to 40 dB in some of the filtering structures.

6.1. Stripline and Broadside Coupled Coplanar Waveguide Launch Structures

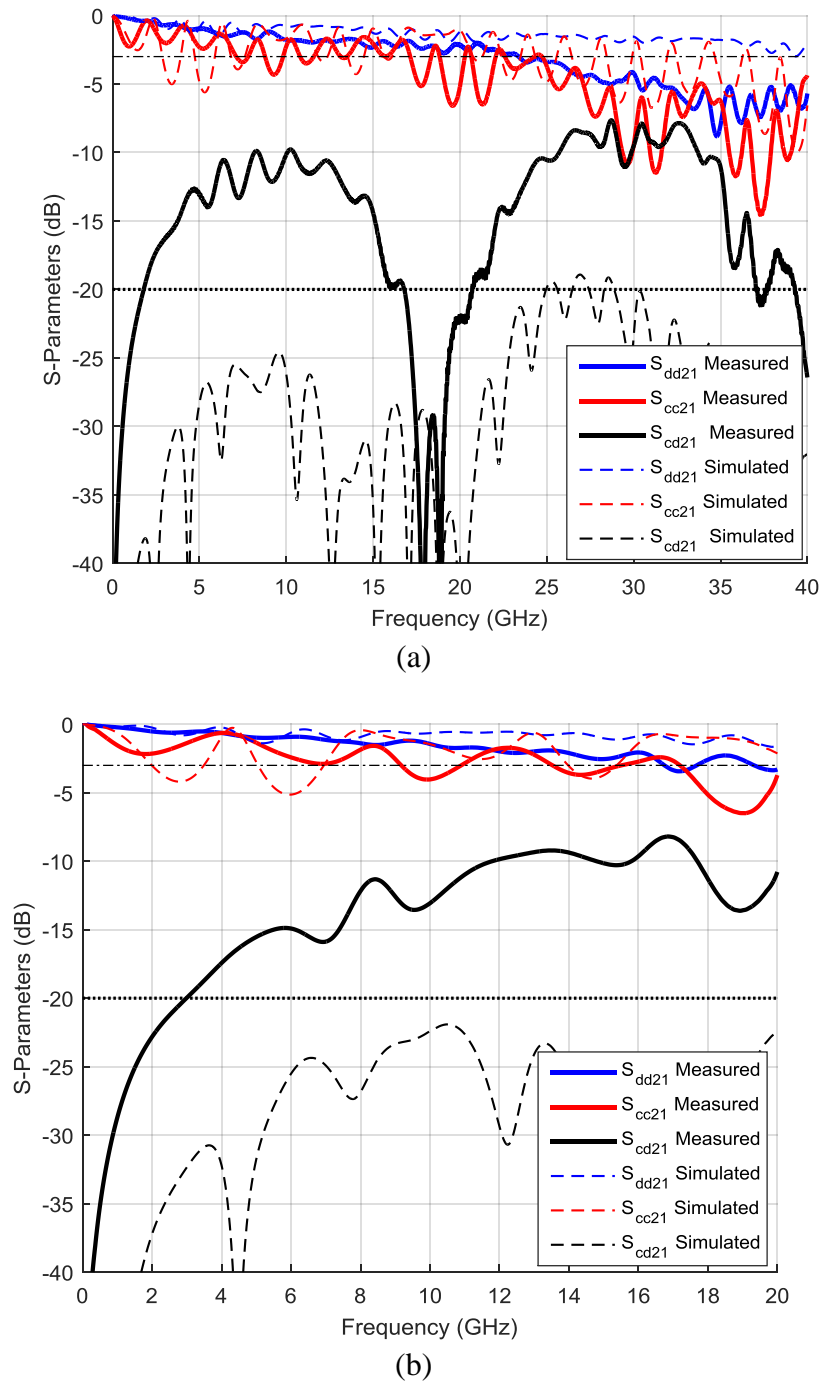
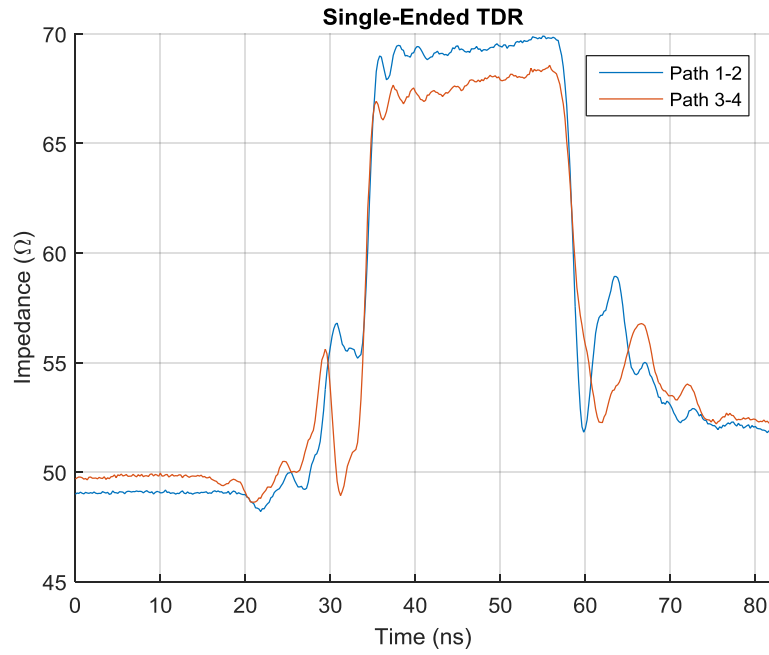


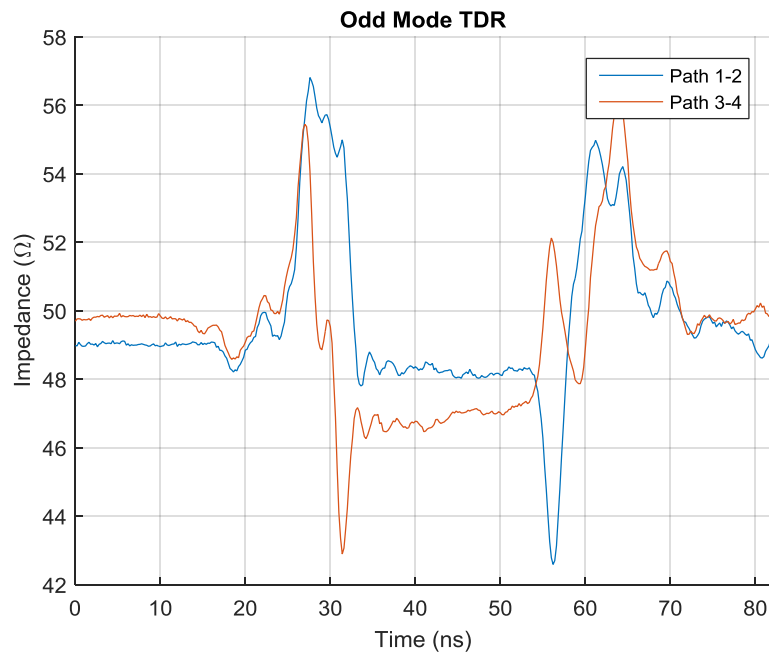
Fig. 6.1 - Measured and simulated S-parameters for a coaxial launched BC-CPW transmission line with no filtering structures and a lengths (a) 5 cm and (b) 2.5 cm. The cross section of the transmission line is shown in Fig. 5.5(c)

Fig. 6.1 shows measured and simulated results for two traces with no filtering elements, one is a 5 cm long transmission line and the other is 2.5 cm long. The differential transmission stays above -3 dB (the black dash-dot line) past 16 GHz in both the 2.5 cm and 5 cm transmission lines. In the 5 cm transmission line, the differential transmission goes below -5 dB at about 30 GHz, the results for the 2.5 cm transmission line are only plotted up to 20 GHz. This differential transmission is worse than predicted by simulation. Some the difference might be accounted for by the non-ideal bolt on coaxial connectors used in measurement versus the ideal coaxial connectors used in simulation. Overall the differential transmission survives fairly well over a broad range of frequencies.

In the simulated results the CM conversion stays below -20 dB (the thicker black dotted line) in both the short and long trace. Since the CM conversion maxes out at about the same level in both the 5 cm and 2.5 cm traces (note that Fig. 6.1(b) only shows up to 20 GHz), it is most likely that the majority of the CM conversion is introduced by the launch structure. In the measured results, the CM conversion is much higher, maxing out at above -10 dB. This difference is very concerning as introduced CM energy is extremely counterproductive to the goal of using this structure to transition to CM filters that eliminate CM energy. In an attempt to identify the source of the difference between, the impedance of the 5 cm traces were measured using a time domain reflectometer.



(a)



(b)

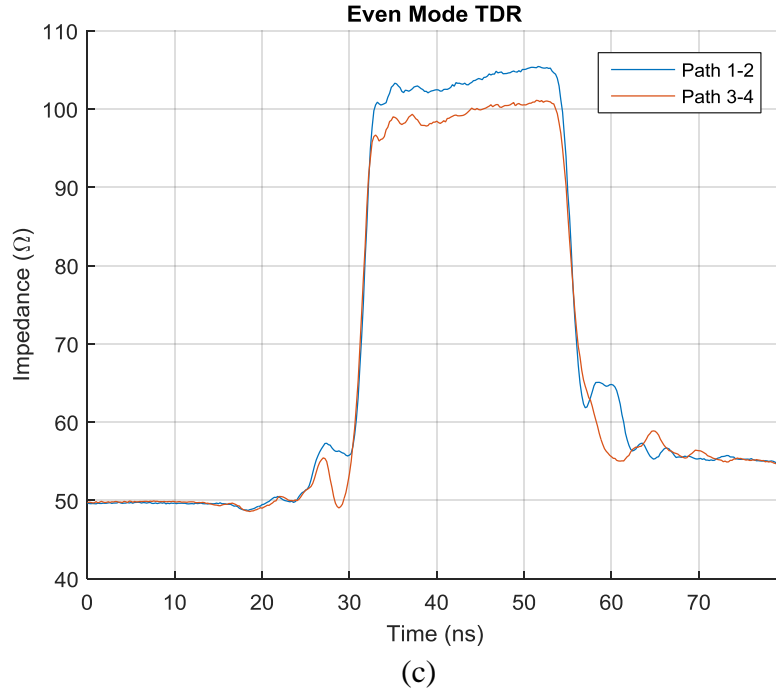
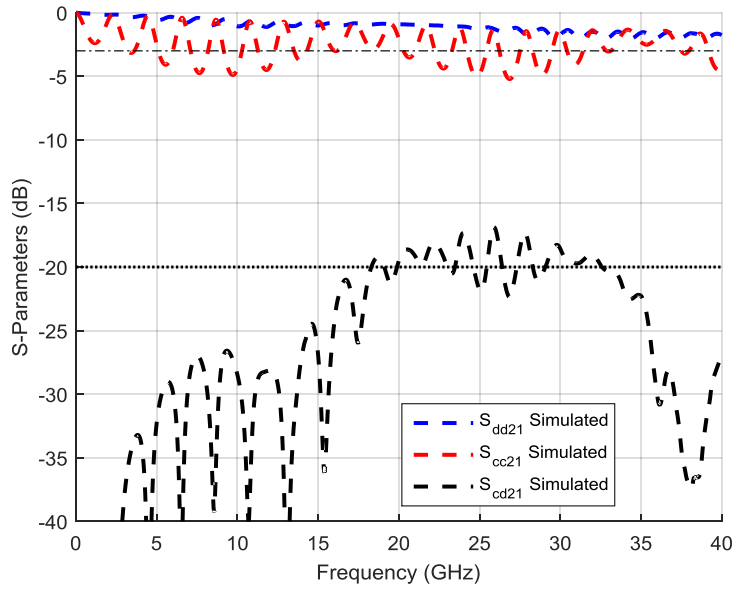


Fig. 6.2 - Measured (a) single-ended, (b) odd mode, and (c) even mode time domain reflectometer signals using the coaxial launch structure with no filtering structure.

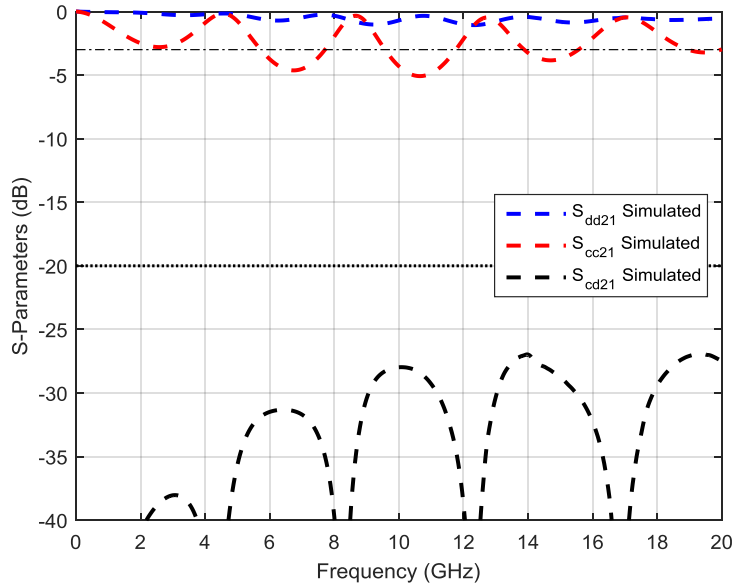
Fig. 6.2(b) shows that the odd mode impedance is about 48Ω , throughout the transmission line. More importantly for identifying sources of measured CM conversion, the length of the traces seem very similar. The falling edges of path 1-2, the path that does not have a via transition, and path 3-4, which does have a via transition, in Fig. 6.2(a) and (c) are very close together in time. Unfortunately, at 10 GHz, near where the CM conversion is maximum in the 5 cm line, half a wavelength of phase difference would only result in a time difference of 50 picoseconds. The TDR used has a maximum sampling rate of 20 picoseconds, making half a wavelength of phase difference difficult to see on the measurement and distinguish from jitter. More investigation is needed to identify the sources of the excess CM conversion. This is discussed further in the future work section below.

The RF probe launched BC-CPW trace with no filtering structure was unfortunately unable to be measured due to difficulties with the RF probes. The simulations of the RF probe launched

5 cm and 2.5 cm traces with no filters are shown below in Fig. 6.3. The simulated performance is very similar to the simulated performance of the coaxial launches traces. This is promising since it shows repeatability across different launch methods. It also means that the probe launches will probably also suffer from the same problems as the coaxial launch.



(a)



(b)

Fig. 6.3 - Simulated S-parameters for a RF probe launched BC-CPW transmission line with no filtering structures and a lengths (a) 5 cm and (b) 2.5 cm. The cross section of the transmission line is shown in Fig. 5.5(c)

For the stripline topology, a TRL calibration set was designed into the test board. TRL calibration eliminates the effects of the launch structures on the measurements. TRL calibration is used for the stripline traces since stripline is a common topology and transitions to stripline are commonly implemented by PCB designers. BC-CPW, however, is a new topology that might be limited in usefulness without a practical launch structure. Demonstrating an effective stripline launch is thus less important than demonstrating an effective BC-CPW launch. Nonetheless, simulations of the stripline filters were performed with a model of the stripline launch. This gives flexibility if TRL calibration cannot be performed. The simulated results for filter structures that include the stripline launch are shown in Appendix C in Fig. C.4 through C.7. The differential transmission remains above -1.5 dB from DC to 18 GHz and above -2.5 dB up to 20 GHz. Most of the loss in differential transmission can be attributed to dielectric loss and dispersion, but at frequencies above 18 GHz, there is some ripple that is introduced by the launch structure.

Overall, both stripline and BC-CPW launches perform well in the simulated results. The stripline and RF probe BC-CPW launches have not been tested in measurement. The RF probe launch and the BC-CPW launch perform similarly in simulation and would probably perform similarly in measurement.

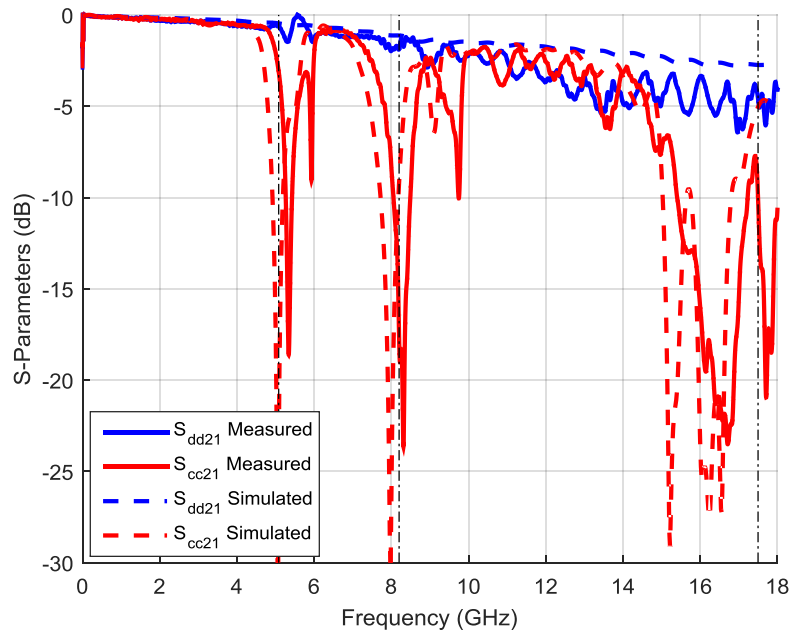
The coaxial BC-CPW launch structures maintain differential transmission of better than -3.5 dB from DC to 20 GHz in measurement. Differential transmission below -3 dB means that more than half of the input power is not coming out on the output. The loss in the transmission line could account for most of the power lost between input and output. The linear (on a dB scale) downward slope of the differential transmission coefficient supports this conclusion since loss increases exponentially with frequency. However, above 30 GHz, ripple becomes more

prevalent in the differential transmission. Ripple is indicative of mismatch and reflection. Looking at the differential reflection, S_{dd11} , reveals that the reflection increases above 30 GHz. CM conversion may also be a source of noticeable loss. The loss in the transmission line cannot be mitigated by the launch structure. Reflection and CM conversion, however, may be introduced by the launch structure. The launch structure could be better optimized to reduce reflection and allow the differential signal to survive better at higher frequencies.

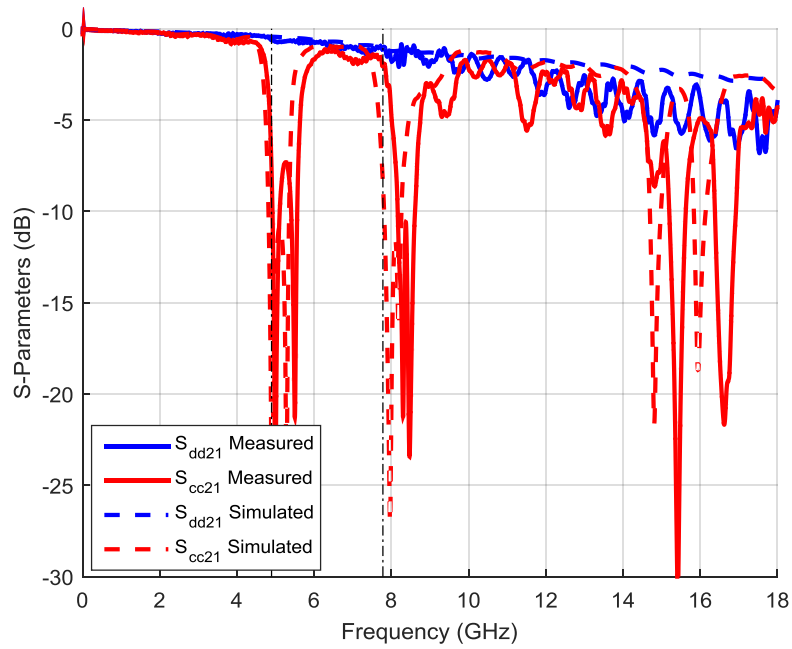
The common mode conversion caused by the BC-CPW launch structure is also a serious concern. The simulations showed common mode conversion, S_{cd21} , being at most -20 dB. In measurement S_{cd21} reaches -10 dB. The filtering structures will eliminate some of the introduced common mode energy, but the transition on the output side will again result in some common mode conversion. The launch structure has many different parameters that may result in increased common mode conversion compared to simulation. A sensitivity analysis of some of those parameters and an analysis of the fabricated structure would help to narrow down the reason for the discrepancy and inform future launch structure designs.

6.2. Microstrip Filter Performance

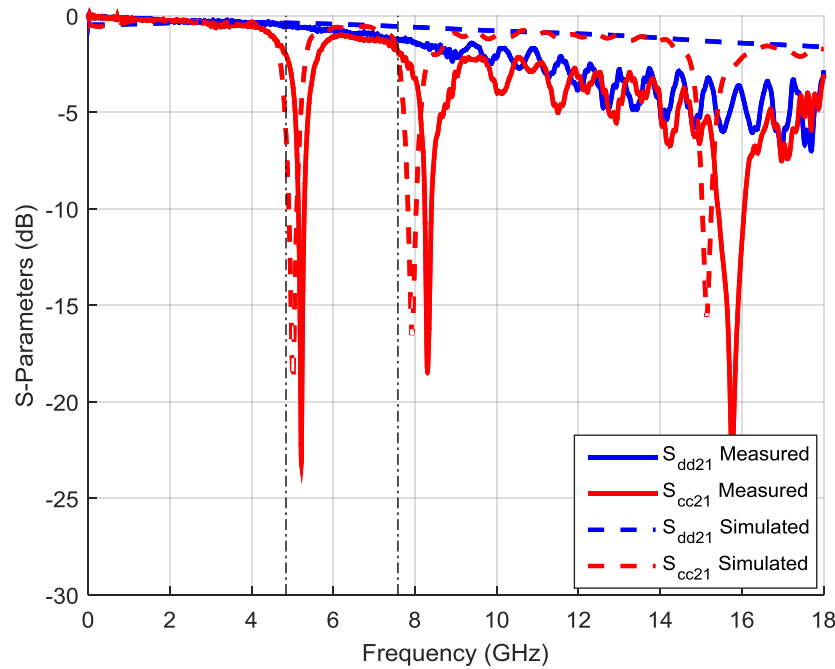
The microstrip filters show effective but relatively narrowband common mode filtering. Fig. 6.4 shows that in each case the CM signal is attenuated by greater than 10 dB and usually by greater than 20 dB. The single filter with a shifted via in Fig. 6.4(c) demonstrates the viability of using the bowtie filter with a dual band operation. The attenuation is not as strong as in symmetric filters, which is expected since the symmetric filter is effectively two cascaded filters operating at the same frequency. The single filter, however, still attenuates the CM signal by about 15 dB, which is probably adequate for most applications.



(a)



(b)



(c)

Fig. 6.4 - Simulated and measured transmission data for (a) three cascaded symmetric filters targeted near 5, 8, and 16 GHz, (b) two cascaded filters with shifted vias targeted near 5 and 8 GHz, and (c) a single filter with a shifted via targeted near 5 and 8 GHz

The differential transmission stays above -3 dB to about 10 GHz but starts to experience ripple at approximately 5 GHz. This ripple is present in the measured results but not in the simulated results, indicating some difference in the model and what was actually fabricated. One potential source of this difference is the transition from the coaxial cable to the microstrip line. The coaxial cable is calibrated out before measurement, but the connector used to transition from coaxial cable to the board is not calibrated out. At low frequencies, this transition is electrically short, resulting in minimal reflection and ripple. As the frequency increases, the length is longer relative to a wavelength and thus more impactful. This makes sense since the ripple increases with frequency and thus shorter wavelengths. The simulation includes an idealized model of this launch which maintains 50Ω impedance throughout, eliminating the ripple-causing mismatch.

In addition to ripple, the differential transmission decays with frequency. The microstrip architecture suffers from higher loss due to radiation than the other architectures explored. Furthermore, the measured differential transmission decays more rapidly than the simulated result at high frequencies. The non-idealities of the coaxial to microstrip transition probably contributes to this, but it could be related to the effective permittivity being different in measurement than in simulation. In the common mode transmission, many features of the results are shifted down in frequency relative to measurement, implying a higher permittivity. A higher permittivity would result in more wavelengths over the same distance. Loss is related to the number of wavelengths traveled. A higher permittivity could contribute to the higher loss seen in measurement versus in simulation.

The frequency differences observed are somewhat explained due to the potential difference in permittivity from simulation to measurement. However, some of the disparity is probably due to variation in fabrication. The resonances are consistently shifted down in frequency across three different traces consisting of a total of six filtering structures. Either there is a systematic bias in the fabrication method or manufacturing variation has less of an effect than the previously discussed differences between simulation and measurement. An analysis of the frequency differences over a greater sample of traces would help to illuminate the effects of manufacturing variation on the structures.

Overall, the microstrip filters perform well with a fairly small footprint. The difference in filtering frequencies from simulation to measurement poses a larger challenge in this architecture than in the other architectures considered since the filters have a narrower stopband than the bowtie filters implemented in the other topologies. Narrower spacing between the filter and trace would help alleviate this problem because narrower spacing would result in tighter

coupling and thus wider stopbands. In the manufacturing process used for the board considered, the minimum spacing requirement is 0.5 mm which limits the spacing and thus coupling of the trace and filter. A process with more resolution would give more flexibility in this case.

6.3. Stripline Filter Performance

Unfortunately, problems with the measurement setup made measurement of the stripline traces impossible. The RF probes used for this measurement need repair before these measurements can be taken. Instead, simulation results are included in Fig. 6.5 for one stripline filter. This simulation produced an estimation of how the stripline filters will perform. Comparison of the measurement and simulation of the BC-CPW structures which were fabricated on the same circuit board give an idea of how the stripline structures will perform relative to simulation. The rest of the simulations of the stripline filters are included in Appendix C.

At each center frequency, the CM signal is attenuated by greater than 20 dB. The -10 dB bandwidths at the two lower frequencies are just over 1 GHz. Near 16 GHz, the bandwidth is enhanced due to it being near the third harmonic of the lowest filtering frequency and because the filters attenuate odd harmonics. Partially because of this enhancement and partially because of the proportional relationship between bandwidth and center frequency, the -10 dB bandwidth is about 3 GHz and the attenuation around the center frequency is nearly 40 dB. The simulation of a single filter targeted near 16 GHz (shown in Fig. C.6 in Appendix C) has about as much attenuation, indicating that the third harmonic of the 5 GHz filter does not have a very significant effect on the maximum attenuation.

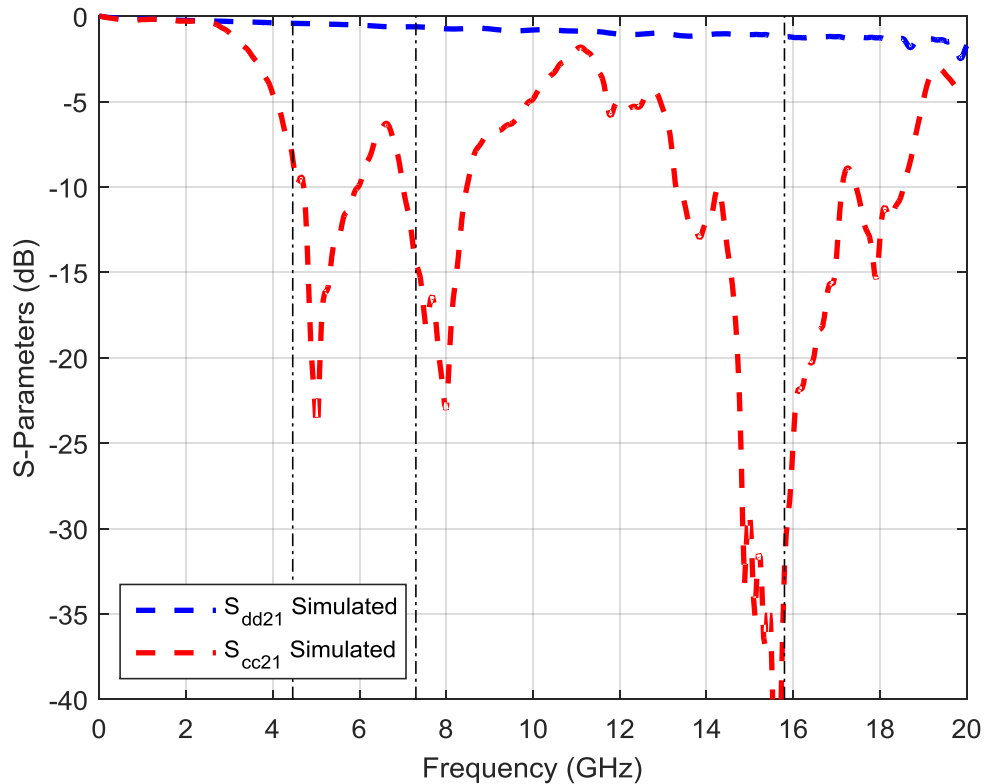


Fig 6.5 - Simulated S-parameter results of three cascaded symmetric filters targeted near 5, 8, and 16 GHz implemented in a stripline topology

6.4. Broadside Coupled Coplanar Waveguide Filter Performance

S-parameter results for four filtering structures in both measurement and simulation are included in this section. Three of the filters are launched with the coaxial launch structure while one is launched with RF probe launch. The results shown are fairly representative of the remaining filtering structures. The results for all BC-CPW filters are included in Appendix C. Due to difficulties with the RF probes; only a single filtering structure was measured with the RF probe launch.

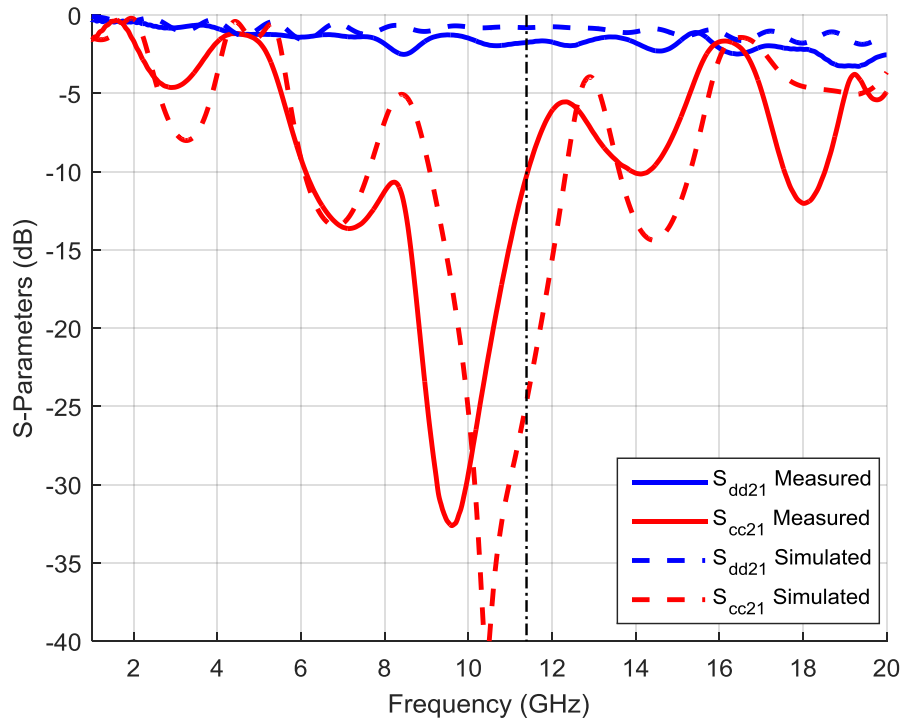


Fig 6.6 - S-Parameter results of coaxial launched broadside coupled filters targeted near 11 GHz

The predicted filtering frequency is 11.4 GHz. The center frequency of the simulated result is 10.7 GHz, while the measured center frequency is much lower at 8.77 GHz. The simulated and measured results have similar shapes, but the measured result is shifted slightly lower in frequency. The much lower center frequency of the measured data is due to the wider stopband compared to the simulated data. This wider stopband is because the measured data does not have quite as much ripple as the simulated data at 8.3 GHz. If that frequency is taken as the edge of the band, the measured result has a center frequency of 9.89 GHz, which is still lower than the simulated data. If the threshold for the stopband is -5 dB instead of -10 dB, then the center frequencies align much more closely at 10.74 GHz simulated and 10.42 GHz measured.

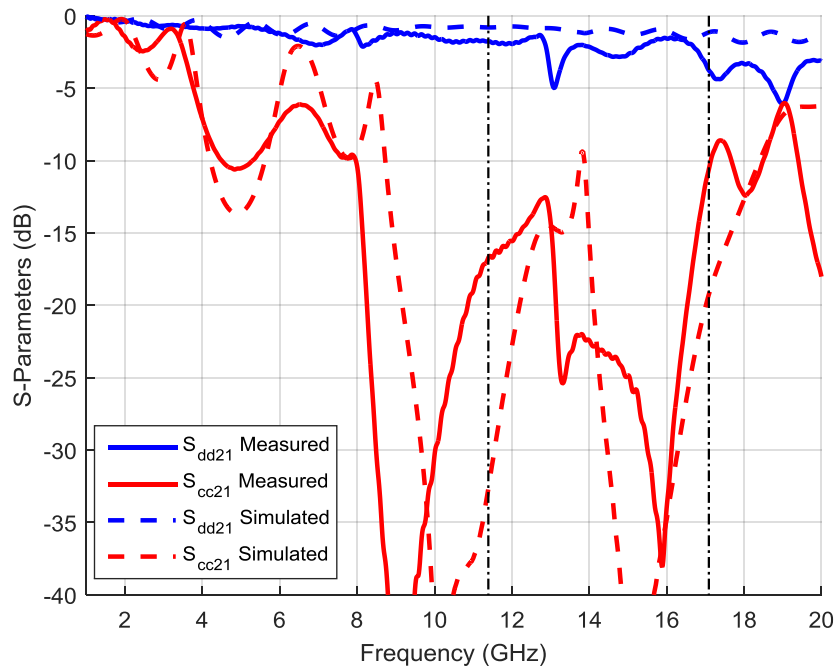


Fig 6.7 - S-Parameter results of coaxial launched broadside coupled filters targeted near 11, and 16 GHz using two cascaded filters

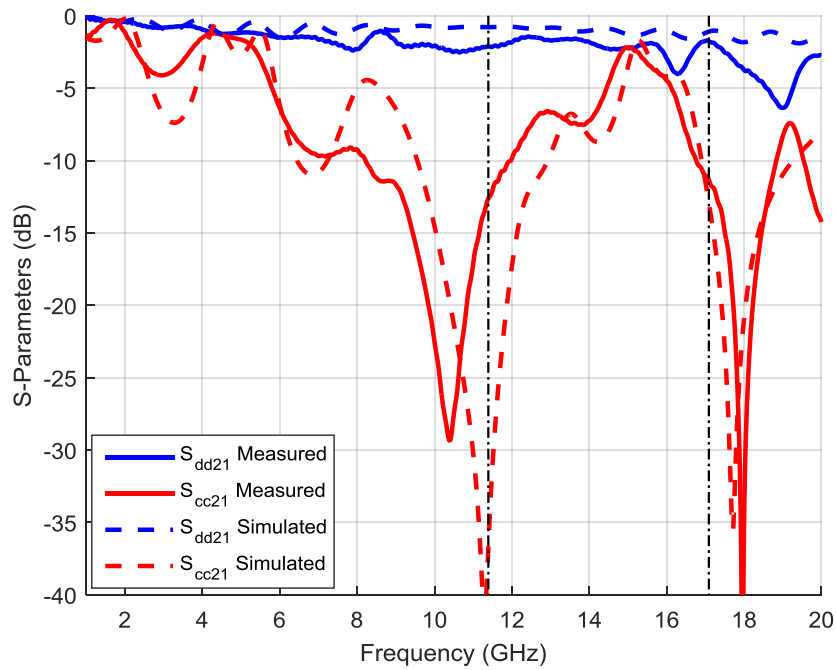


Fig. 6.8 - S-Parameter results of coaxial launched broadside coupled filters targeted near 11 and 16 GHz using a single filter structure

Fig 6.7 shows filtering from two symmetric filters while Fig 6.8 shows multiband filtering from a single asymmetric filter. The filtering in the asymmetric structure does not attenuate as deeply as in the cascaded symmetric filters. This is to be expected since each side of the symmetric filter will filter at the same frequency, while each side of the asymmetric structure filters at a different frequency. The filtering frequencies in the asymmetric filter are also shifted up in frequency slightly relative to the symmetric filters. For example, the center frequency in the band targeted near 11 GHz is 10.7 GHz in the asymmetric filter but is 9.3 GHz in the cascaded symmetric filters. This is possibly due to both sides of the symmetric filter being excited at the same frequency, creating a longer total effective length of the filter, possibly due to interactions between the sides of the filter in the center area between the stubs. In the asymmetric filter, only one side of the filter is excited at a time, reducing the possibility of the sides interacting to effect filtering in the center of the structure.

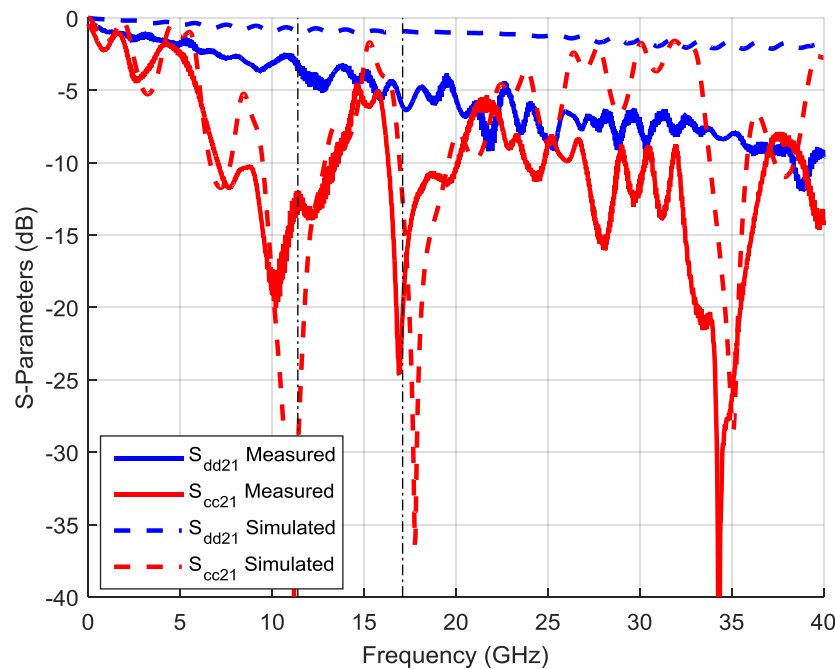


Fig. 6.9 - S-Parameter results of RF probe launched broadside coupled filters targeted near 11 and 16 GHz using a single filter structure

The RF probe launched structure displays filtering at the same lower frequency (10 GHz) as the same structure implemented with the coaxial launch but is shifted downward at the upper targeted frequency (16.9 GHz). The filtering structures are intended to be identical other than the launch structures, and the simulated frequencies match nearly exactly. This could give some indication of the effect that process variation can have on the filtering frequency even on the same test board. These two traces were oriented in opposite directions on the board which supports the possibility of process variation, but, the RF probe measurement has not been validated through a second measurement on a different instrument, so we cannot be thoroughly confident of the RF probe measurements shown. The filtering is not as deep in the RF probe launched structure, but again, since the measurement has not been validated, it could be an artifact of measurement.

In all of the BC-CPW filters, as with the filtering structures in the previously considered topologies, the measured and simulated results show some discrepancies. Features in the measured common mode transmission data are shifted down in frequency relative to the analogous features in the simulated data. This is consistent across nearly all the BC-CPW filtering structures. The frequency shift is due to differences between the simulated structure and the physical device. The shift in frequency could possibly be attributed to the manufactured board being slightly thinner than modeled. A thinner board would result in the traces coupling more strongly to the filters, shifting filtering down in frequency. It would also change the effective permittivity and thus the velocity of propagation in the devices. Specifically, tighter coupling created by a thinner board would increase the effective permittivity as more of the flux would be confined in the dielectric as opposed to air. An increase in effective permittivity relative to simulation would result in a downward frequency shift as compared with simulation.

More work is needed to identify the source of the frequency differences precisely. Additional steps that can be taken to narrow down the origin of the disparity are discussed in the Future Work section below.

Every BC-CPW filter shows strong common mode attenuation within the common mode stop band. All filtering structures are also relatively broadband when compared with the edge-coupled filters in microstrip and stripline architectures. For example, the single 8 GHz broadside coupled filter has a -10 dB bandwidth of approximately 2.5 GHz which is greater than a 30% bandwidth. The 8 GHz filter implemented in stripline has a -10 dB bandwidth of approximately 1.5 GHz which is a bandwidth of about 20%. Additionally, the maximum attenuation of the broadside coupled filter is greater than 40 dB while the maximum attenuation in the edge-coupled stripline filter is about 20 dB. This matches the expectation that stronger coupling corresponds to stronger and broader band filtering.

The differential transmission measured in the filtering structures is in line with the differential transmission measured in a trace without a filter which supports the prediction that adding a filter to a BC-CPW trace would not have an effect on the differential transmission.

7. LIMITATIONS

The bowtie filter is fairly easy to implement in the topologies as described. Implementation may be more difficult in other differential transmission lines or in different layouts of the topologies described. For example, the differentially coupled transmission lines used in this implementation have enough room for the filter and via in between. If the traces are closer together, the filter cannot be placed in between them without some adjustment to the path of the traces which could have other effects. The stripline and BC-CPW implementations use a stackup with three metallization layers. This is rarely used in practice. A four-layer stackup would be incompatible with the BC-CPW topology since it would result in one trace being partially in air while the other trace would be entirely surrounded by dielectric.

For filtering at low frequencies, the bowtie filters are impractical due to the size needed. This is generally a problem with microwave filters since the size of the filter is often proportional to the filtered wavelength. The proportionality along with the inverse proportionality of wavelength and frequency limits the bowtie filter to frequencies in the gigahertz range, since the filter may be prohibitively long at low frequencies. If, however, a long length of differential transmission line is needed anyway, implementing the bowtie filter could be practical, since the length needed already exists, and the width can be very small. For filtering at very high frequencies, very small filters are needed. As the filter becomes smaller, manufacturing process variation will have a larger relative impact on the filtering frequency.

The filters are further limited by the needed signal launches. In particular, the signal launches are the limiting factor in practical implementation of the BC-CPW topology. The design examined has a maximum measured common mode conversion of around -10 dB between DC and 40 GHz. This may be unacceptably high in some applications as it means about 10% of

the differential energy is converted to common mode. Additionally, the difference between the simulated and measured results indicate that the launch structure is difficult to model or is sensitive to manufacturing variations. In either case, it reduces the predictability and repeatability of the structure which is undesirable in a practical implementation that might require repeatability over a large number of devices. Finally, the signal launch limits the frequency range in both the stripline and BC-CPW topologies. Both BC-CPW and stripline architectures can perform adequately well into mm-wave frequencies. However, the launch structures investigated can only function well up to the lower edge of the mm-wave band. A better launch structure would enable operation at higher frequencies. Existing applications operate within the frequency range of the launch structures, but future applications will make use of higher frequencies and will need launch structures that can serve those frequencies.

8. FUTURE WORK

First of all, the remainder of the RF probe launched structures, both BC-CPW and stripline, must be measured. The work already accomplished shows that these filtering structures can accomplish effective common mode filtering and that the filters can be made practical through differential signal launches. Further work is needed in characterizing the BC-CPW structure and the launch structures including sensitivity analyses, as well as in creating more general and accurate design equations for the filtering structures. Examination of the sources of differences between measurement and simulation is needed to inform both simulation and fabrication and to reconcile the discrepancies. The presence of common mode conversion in the measurement of the BC-CPW launch structures that were not present in simulation is especially worrisome as the purpose of the launch structures is to allow for common mode filtering. Introducing common mode energy undermines the purpose of the structures. Finally, an investigation into using bowtie filters in multilayer boards may be needed to fully realize the practicality and applicability of the filter.

The BC-CPW topology is an extension of the MSTL topology. The MSTL topology is relatively new and is still under investigated. Limited design equations exist for this topology, making designing for specific impedances with some dimensions held constant difficult. Extensive simulation and modification must be performed in order to obtain the desired characteristic impedance while maintaining the low dispersion trait that makes the topology useful. In order to design the bowtie filters, the velocity of propagation is needed. The lack of accurate effective permittivity models make this difficult to determine. Additionally, the mixed-mode propagation velocities in the BC-CPW are different than the single-ended propagation

velocity in the MSTL, requiring further investigation into even and odd mode transmission characteristics.

The signal launches and via transitions are important to making the filtering structures practical. The presence of common mode conversion in the measured results of the BC-CPW launches that is not present in simulation must be investigated in order to reduce the CM conversion in future designs. Dimensional analysis of the manufactured board would enable an “as is” simulation that would hopefully give results that more closely match the results measured. Another key to identifying the origin of the difference is a sensitivity analysis of various parameters of the launch structure. The sensitivity analysis can help focus research into the differences between the fabricated and simulated structures, guide design of subsequent BC-CPW launch structures, and assist in the characterization of the various parts of the launch structure.

The via transitions specifically are not well characterized when it comes to propagation velocity or impedance. A model of the transition would be useful, for both the BC-CPW and stripline launches, in adapting the launch to other situations that may have different board thicknesses or dielectric constants. The current structures are only intended for three-layer boards. In practice, three-layer boards are very rarely used. The structures could potentially be adapted to enable the use of the BC-CPW or stripline structures in a six or more layer board. The signal launches could also be adapted to operate up to higher frequencies, since the topologies they are designed for are capable of transmission at higher frequencies. This will require significant additional effort to identify the shortcomings of the current designs and compensate in practical ways to fully utilize the higher frequencies at which the BC-CPW and stripline topologies are effective.

The current design equations are acceptable for an initial estimate. In microstrip and stripline topologies, the stopband can be narrow so a slight discrepancy between predicted and actual filtering frequencies can result in minimal filtering at the frequency it is needed. The existing design equations do not take into account coupling between the traces and the filters which can shift the filtering frequency away from the expected. Simulation sweeps can be done to identify and characterize the effects of different coupling strengths on the filtering frequency.

Finally, the EMC characteristics of the filters themselves can be investigated. The filters prevent common mode energy from propagating and potentially radiating and harming EMC, but the filters themselves may have negative EMC consequences if they radiate the energy coupled by common mode signals. Further research could focus on examining the EMC characteristics of the bowtie filters in the different signal topologies. This would probably be done in simulation by looking at the near and far fields that could couple into other traces creating crosstalk and impairing EMC.

9. CONCLUSION

Effective filtering has been demonstrated with different bowtie filtering structures in three transmission line topologies. This includes asymmetric bowtie filters that can achieve multiband filtering. The new differential topology, BC-CPW, was shown to enable very strong common mode filtering over a wide frequency band with the tradeoff of needing a complex launch structure. The topology also has better differential transmission to higher frequencies than microstrip or stripline. Launch structures have been designed and shown to provide good differential mode transmission from DC to 20 GHz. The launch structures enable practical implementation of the new BC-CPW topology and measurement of filtering structures in a stripline topology.

The BC-CPW launch structure transmits the differential signal adequately, but it still needs refinement to realize the high frequency potential of the BC-CPW topology. While the simulation performs well into mm-wave frequencies, measurement shows that the structure suffers from high CM conversion and high loss into the mm-wave band. An analysis of the fabricated board can be done to identify differences between the simulated model and what was actually made. The data obtained can then inform sensitivity analyses to determine the causes of the high CM conversion. Understanding the reason for the CM conversion can help in understanding how to mitigate it. Ultimately, the BC-CPW transmission line architecture will not be implemented in a practical setting without a low CM conversion launch structure that can transition from a stripline or microstrip topology to the multilayer BC-CPW architecture.

REFERENCES

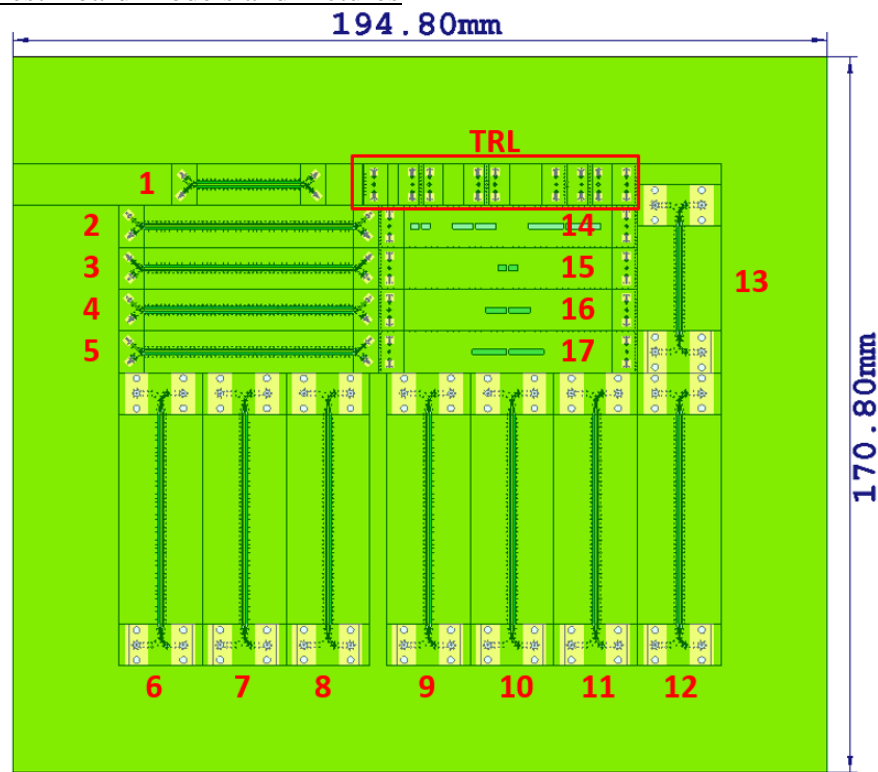
- [1] D. Pozar, *Microwave Engineering*, Hoboken, NJ: Wiley, 2012.
- [2] J. Song and E. Wheeler, *Signal Integrity in Digital Systems: Principles and Practices*, CRC PR I Llc, 2014.
- [3] F. Fesharaki, T. Djerafi, M. Chaker, and K. Wu, "Mode-selective transmission line for DC-to-THz super-broadband operation," in *2016 IEEE MTT-S International Microwave Symposium (IMS)*, San Francisco, CA, July 2016.
- [4] F. Martìn, *Artificial Transmission Lines for RF and Microwave Applications*, Hoboken, NJ: Wiley, 2015.
- [5] W.-T. Liu, C.-H. Tsai, T.-W. Han, and T.-L. Wu, "An Embedded Common mode Suppression Filter for GHz Differential Signals Using Periodic Defected Ground Plane," *IEEE Microwave and Wireless Components Letters*, vol. 18, no. 4, pp. 248-250, April 2008.
- [6] Q. Liu, G. Li, V. Khilkevich, and D. Pomerence, "Common mode Filters With Interdigital Fingers for Harmonics Suppression and Lossy Materials for Broadband Suppression," *IEEE Transactions on Electromagnetic Compatibility*, vol. 57, no. 6, pp. 1740-1743, Dec. 2015.
- [7] F. d. Paulis, M. Cracraft, D. D. Febo, M. H. Nisanci, S. Connor, B. Archambeault, and A. Orlandi, "EBG-Based Common mode Microstrip and Stripline Filters: Experimental Investigation of Performances and Crosstalk," *IEEE Transaction on Electromagnetic Compatibility*, vol. 57, no. 5, pp. 996-1004, Oct. 2015.
- [8] S.-J. Wu, C.-H. Tsai, T.-L. Wu, and T. Itoh, "A Novel Wideband Common mode Suppression Filter for Gigahertz Differential Signals Using Coupled Patterned Ground Structure," *IEEE Transactions on Microwave Theory and Techniques*, vol. 57, no. 4, pp. 848-855, April 2009.
- [9] H.-C. Chen, C.-H. Tsai, and T.-L. Wu, "A Compact and Embedded Balanced Bandpass Filter With Wideband Common mode Suppression on Wireless SiP," *IEEE Transactions on Components, Packaging and Manufacturing Technology*, vol. 2, no. 6, pp. 1030-1038, June 2012.
- [10] A. Fernández-Prieto, J. Martel, J. S. Hong, F. Medina, S. Qian, F. Mesa, and F. Martín, "Differential transmission line for common mode suppression using double side MIC technology," in *2011 41st European Microwave Conference*, Manchester, 2011.
- [11] C.-H. Wu, C.-H. Wang, and C. H. Chen, "Novel Balanced Coupled-Line Bandpass Filters With Common mode Noise Suppression," *IEEE Transactions on Microwave Theory and Techniques*, vol. 55, no. 2, pp. 287-295, Feb. 2007.

APPENDICES

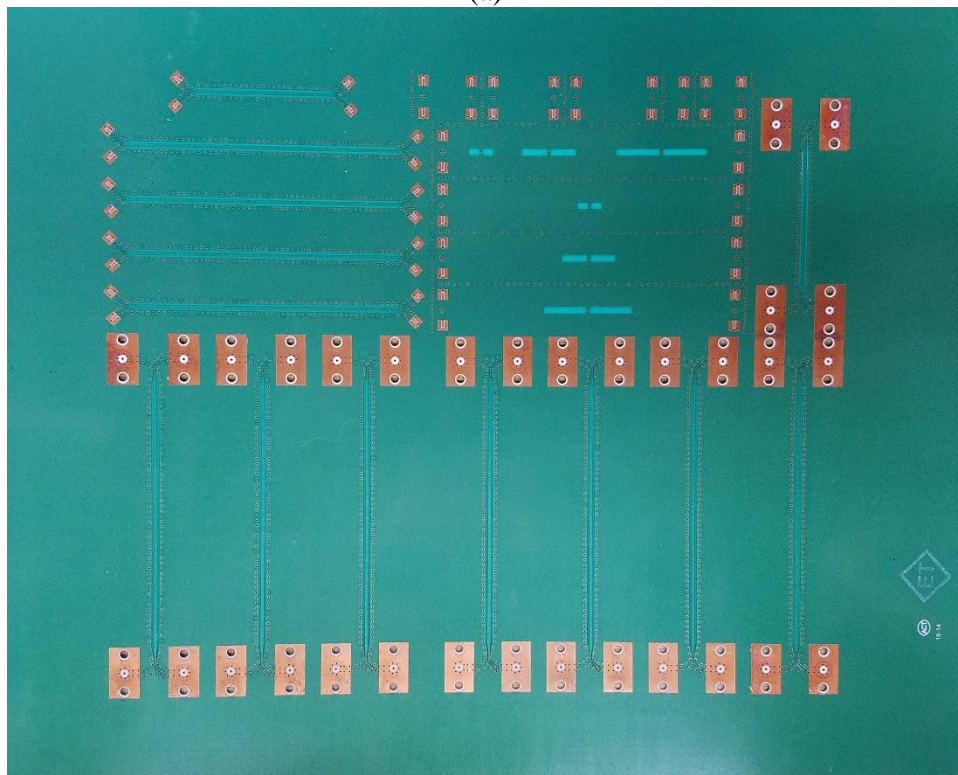
Appendix A: Single-Ended to Mixed-Mode S-Parameter Conversions

$S_{dd11} = 1/2 (S_{11} - S_{13} - S_{31} + S_{33})$	(I.1a)
$S_{dd12} = 1/2 (S_{12} - S_{14} - S_{32} + S_{34})$	(I.1b)
$S_{dd21} = 1/2 (S_{21} - S_{41} - S_{23} + S_{43})$	(I.1c)
$S_{dd22} = 1/2 (S_{22} - S_{42} - S_{24} + S_{44})$	(I.1d)
$S_{cd11} = 1/2 (S_{11} + S_{31} - S_{13} - S_{33})$	(I.1e)
$S_{cd12} = 1/2 (S_{12} + S_{32} - S_{14} - S_{34})$	(I.1f)
$S_{cd21} = 1/2 (S_{21} + S_{41} - S_{23} - S_{43})$	(I.1g)
$S_{cd22} = 1/2 (S_{22} + S_{42} - S_{24} - S_{44})$	(I.1h)
$S_{dc11} = 1/2 (S_{11} + S_{13} - S_{31} - S_{33})$	(I.1i)
$S_{dc12} = 1/2 (S_{12} - S_{32} + S_{14} - S_{34})$	(I.1j)
$S_{dc21} = 1/2 (S_{21} - S_{41} + S_{23} - S_{43})$	(I.1k)
$S_{dc22} = 1/2 (S_{22} - S_{42} + S_{24} - S_{44})$	(I.1m)
$S_{cc11} = 1/2 (S_{11} + S_{13} + S_{31} + S_{33})$	(I.1n)
$S_{cc12} = 1/2 (S_{11} + S_{13} + S_{31} + S_{33})$	(I.1p)
$S_{cc21} = 1/2 (S_{11} + S_{13} + S_{31} + S_{33})$	(I.1q)
$S_{cc22} = 1/2 (S_{11} + S_{13} + S_{31} + S_{33})$	(I.1r)

Appendix B: Test Board Models and Pictures



(a)



(b)

Fig B.2 - Test board (a) CST computer model and (b) fabricated version

Table B.1

Structure Number	Filter Implemented
Probe Launched BC-CPW:	
1	2.5 mm TL w/ no filter
2	5 mm TL w/ no filter
3	Cascaded 8, 11, and 16 GHz filters
4	Cascaded 11 and 16 GHz filters
5	Single 11 and 16 GHz filter
Coaxial Launched BC-CPW:	
6	Single 11 and 16 GHz filter
7	Cascaded 11 and 16 GHz filters
8	Single 16 GHz filter
9	Single 11 GHz filter
10	Single 8 GHz filter
11	Cascaded 8, 11, and 16 GHz filters
12	5 mm TL w/ no filter
13	2.5 mm TL w/ no filter
Probe Launched Stripline:	
14	Cascaded 5, 8, and 11 GHz filters
15	Single 11 GHz filter
16	Single 8 GHz filter
17	Single 5 GHz filter

Appendix C: S-Parameter Results for All Filter Structures
Microstrip:

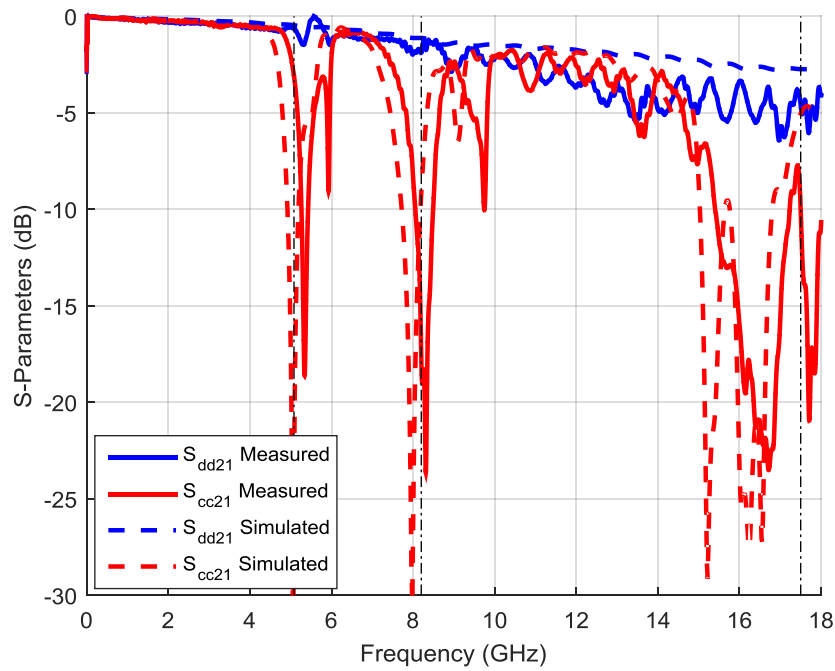


Fig. C.1 - Three cascaded symmetric filters with quarter wavelength L1, L2, and L3.
 L1 = 8.6 mm (5.08 GHz), L2 = 5.0 mm (8.20 GHz), L3 = 1.9 mm (17.48 GHz)

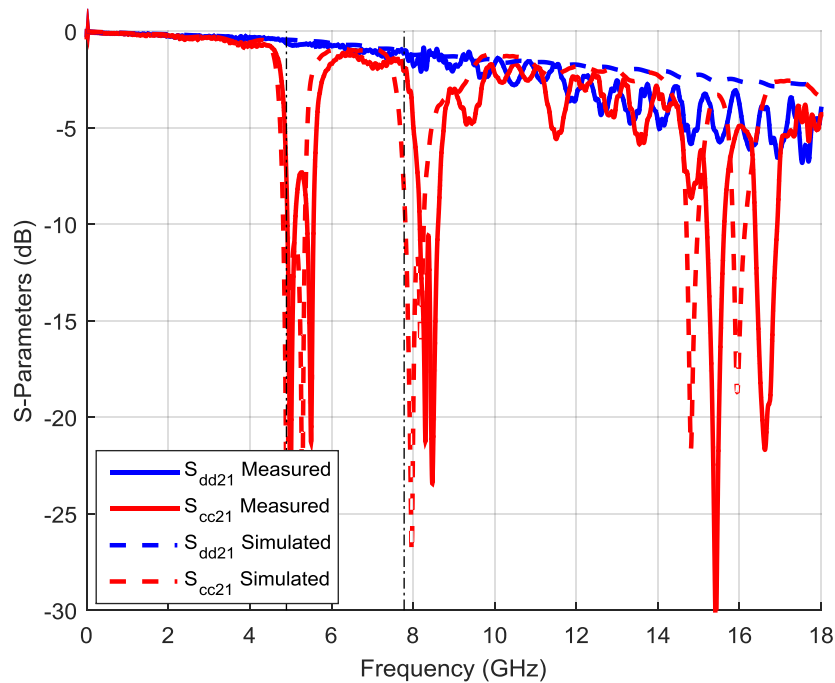


Fig. C.2 - Two cascaded asymmetric filters. Filter 1 has quarter wavelengths of L1 and L2.
 Filter 2 has quarter wavelengths of L3 and L4.
 L1 = 8.6 mm (5.08 GHz), L2 = 5.5 mm (7.55 GHz),
 L3 = 5.31 mm (7.78 GHz), L4 = 9.35 mm (4.71 GHz)

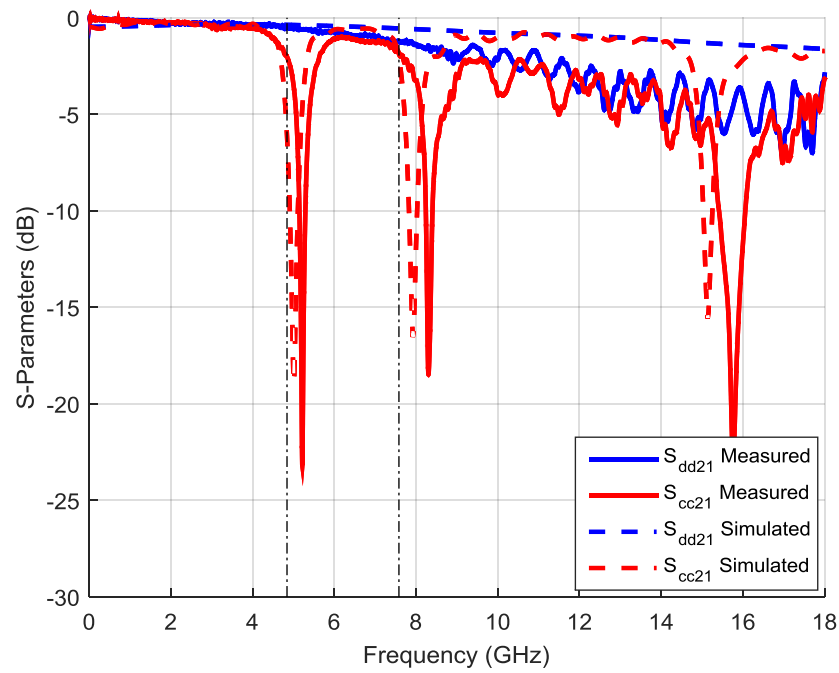


Fig. C.3 - Single asymmetric filter with quarter wavelengths of L1 and L2.
L1 = 9.06 mm (4.84 GHz), L2 = 5.47 mm (7.58 GHz)

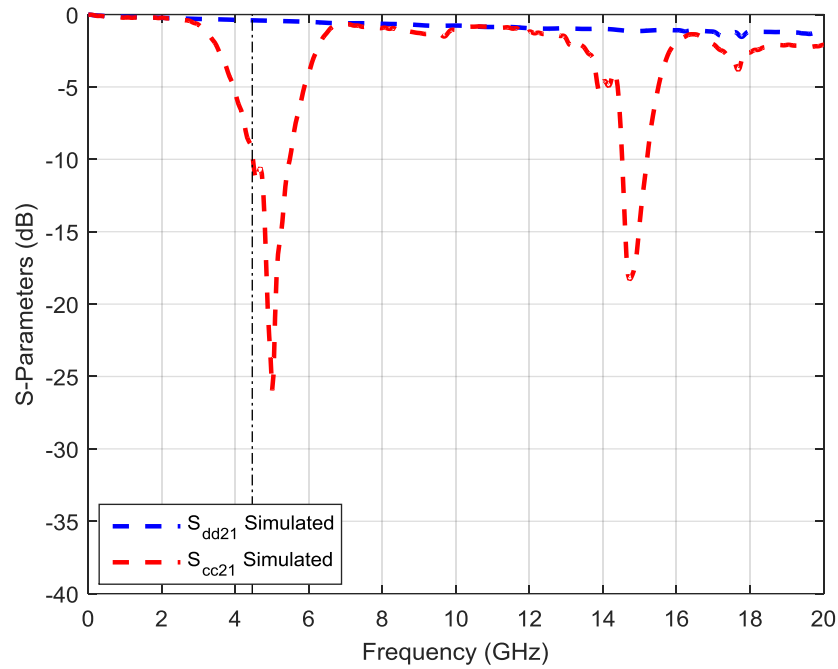
Stripline:

Fig. C.4 - Single symmetric filter with quarter wavelength of L1. L1 = 8.37 mm (4.46 GHz)

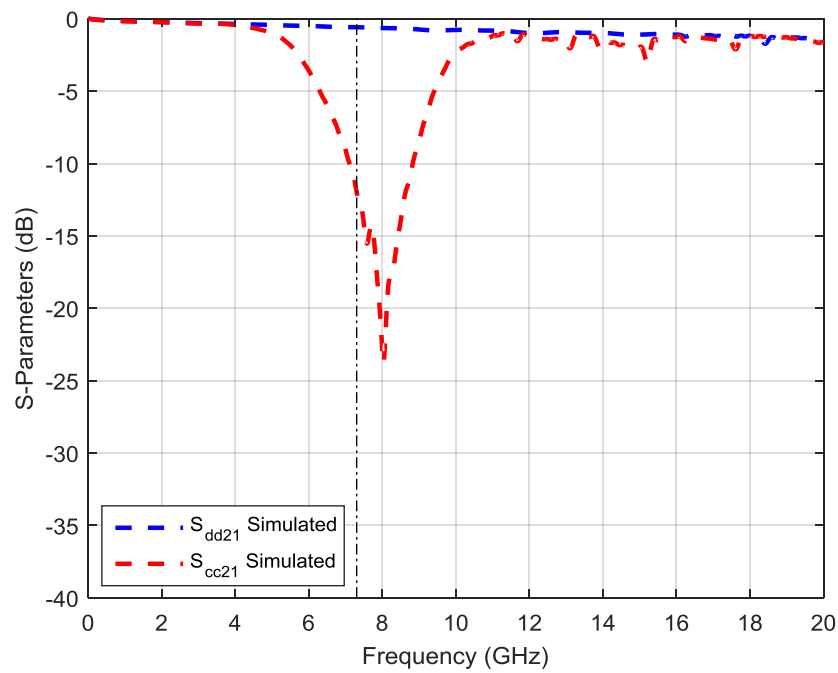


Fig. C.5 - Single symmetric filter with quarter wavelength of L1. L1 = 4.96 mm (7.30 GHz)

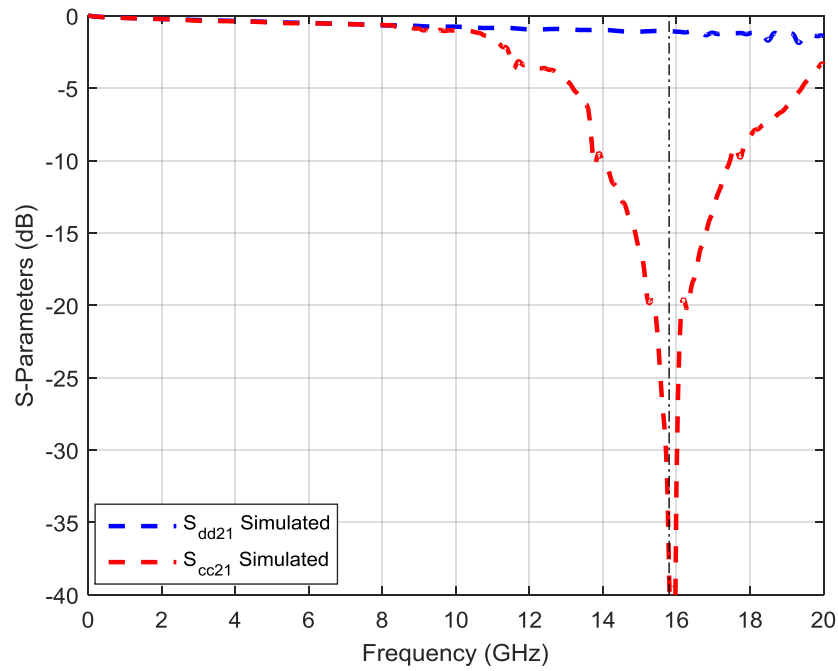


Fig. C.6 - Single symmetric filter with quarter wavelength of L1. L1 = 2.08 mm (15.8 GHz)

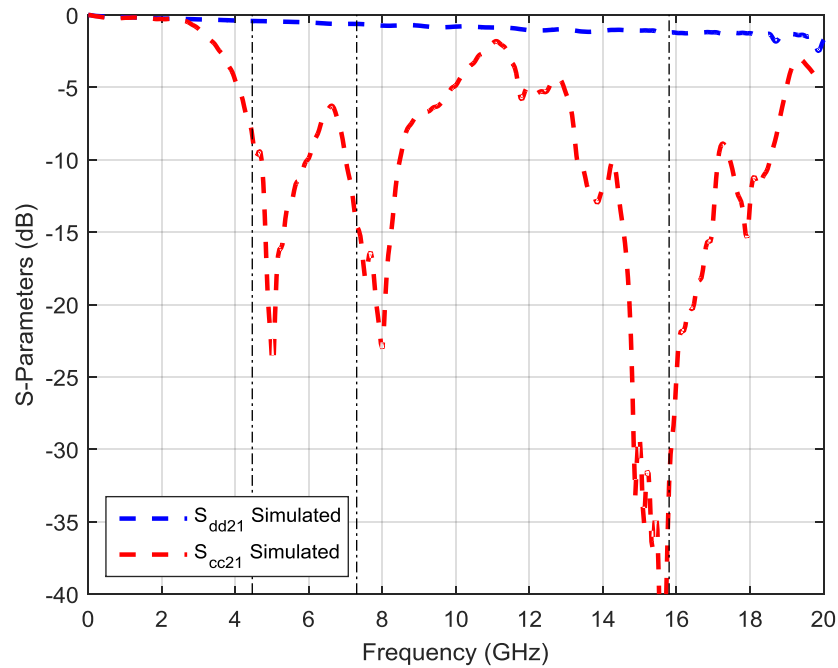


Fig. C.7 - Three cascaded symmetric filters with quarter wavelengths of L1, L2, and L3.
L1 = 8.37 mm (4.46 GHz), L2 = 4.96 mm (7.30 GHz), L3 = 2.08 mm (15.8 GHz)

BC-CPW Coaxial Launch:

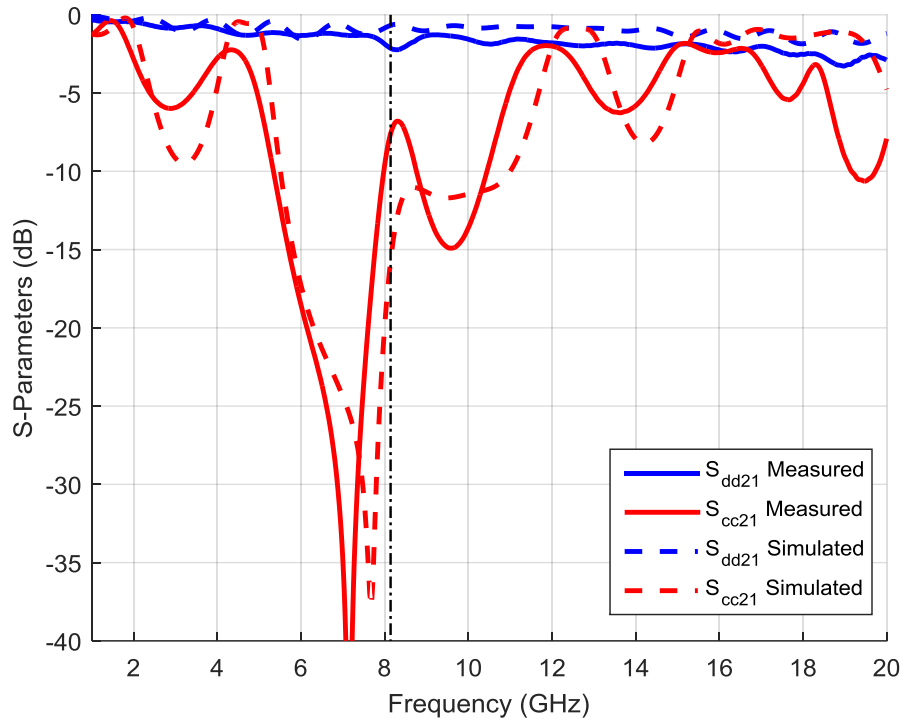


Fig. C.8 - Single symmetric filter with quarter wavelength L_1 . $L_1 = 4.31$ mm (8.14 GHz)

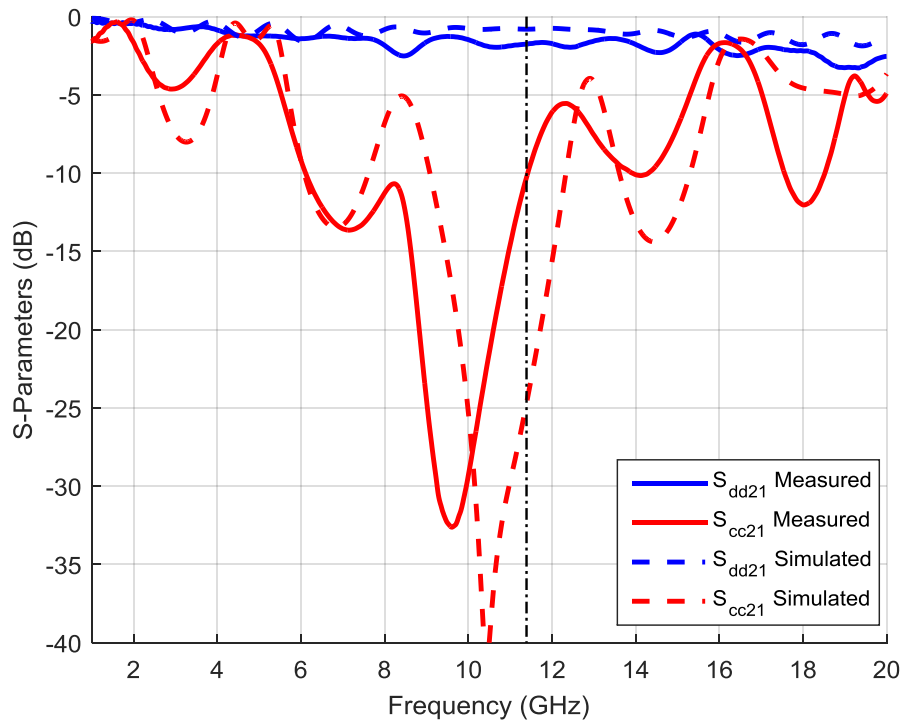


Fig. C.9 - Single symmetric filter with quarter wavelength L_1 . $L_1 = 2.93$ mm (11.4 GHz)

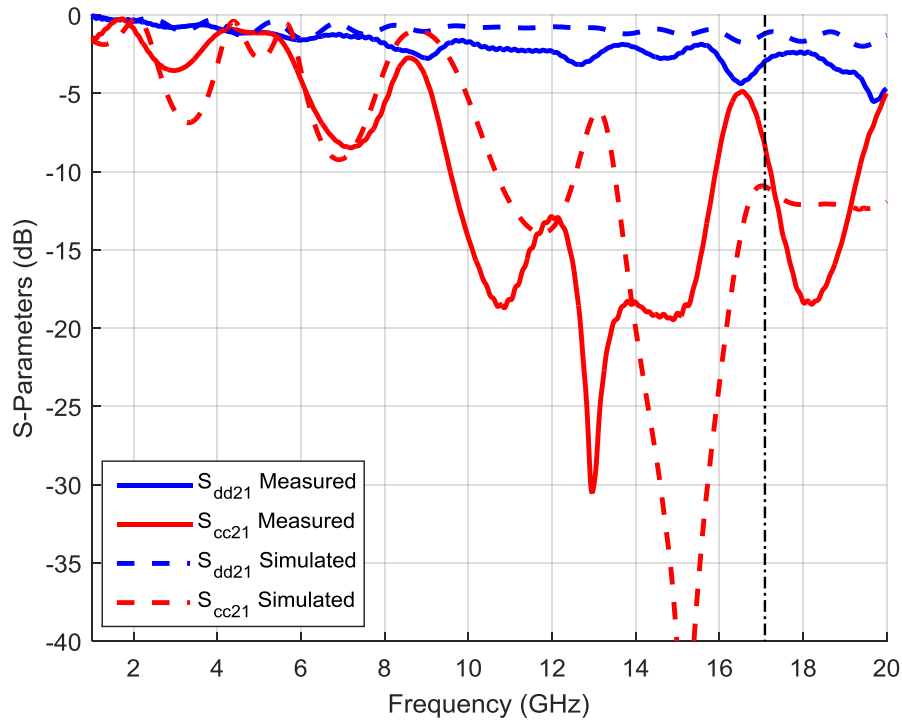


Fig. C.10 - Single symmetric filter with quarter wavelength L_1 . $L_1 = 1.79$ mm (17.1 GHz)

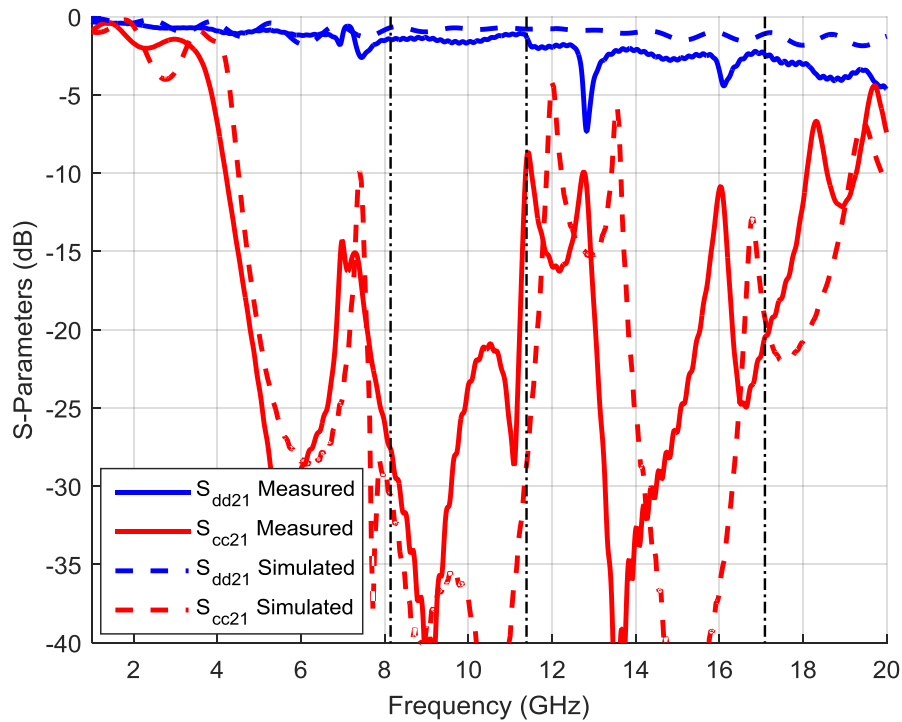


Fig. C.11 - Three cascaded symmetric filters with quarter wavelengths L_1 , L_2 , and L_3 . $L_1 = 4.31$ mm (8.14 GHz), $L_2 = 2.93$ mm (11.4 GHz), $L_3 = 1.79$ mm (17.1 GHz)

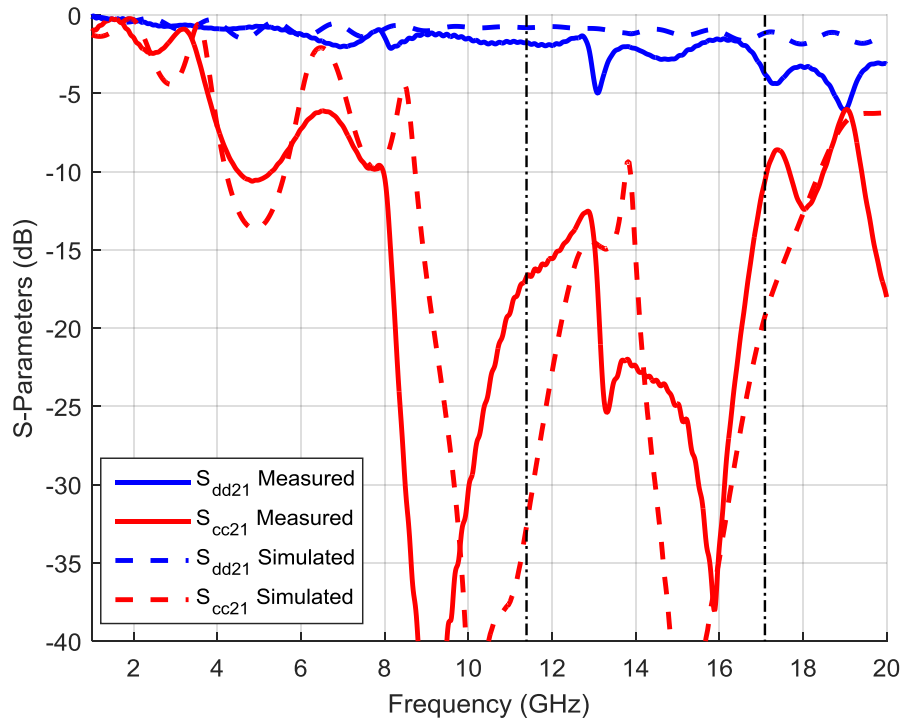


Fig. C.12 - Two cascaded symmetric filters with quarter wavelengths L1 and L2.
L1 = 2.93 mm (11.4 GHz), L2 = 1.79 mm (17.1 GHz)

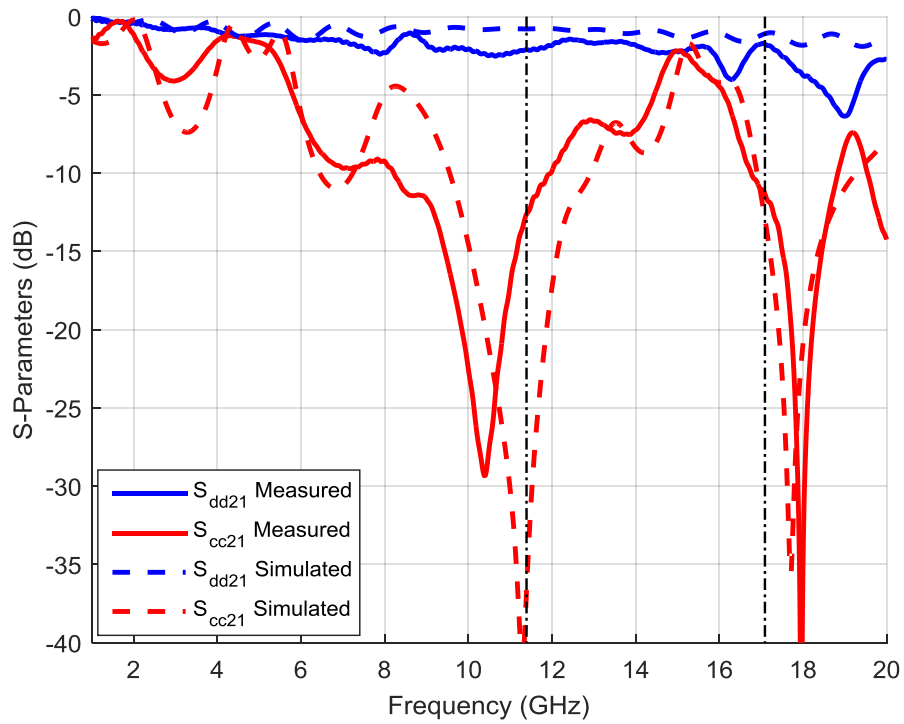


Fig. C.13 - Single asymmetric filter with quarter wavelengths L1 and L2.
L1 = 2.93 mm (11.4 GHz), L2 = 1.79 mm (17.1 GHz)

BC-CPW RF Probe Launch:

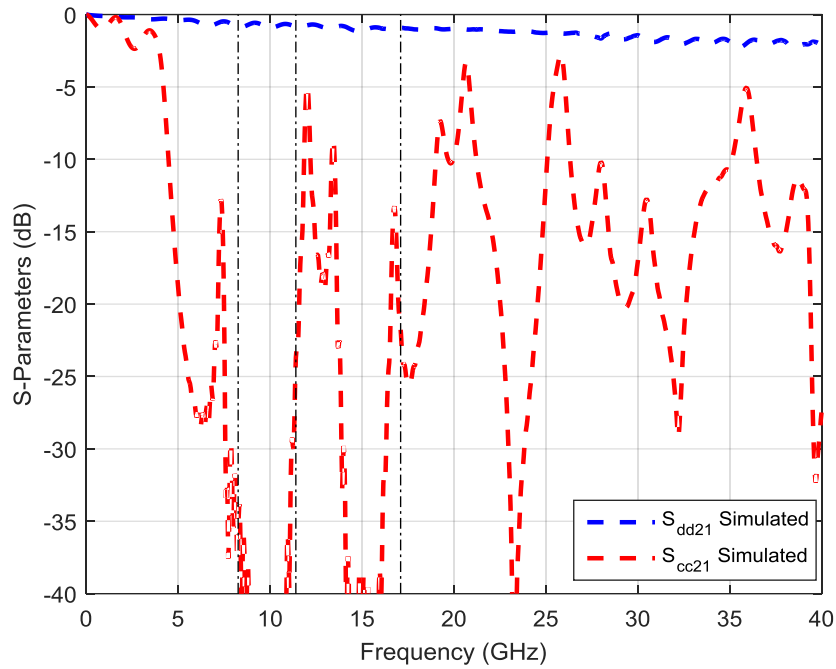


Fig. C.11 - Three cascaded symmetric filters with quarter wavelengths L1, L2, and L3.
 L1 = 4.31 mm (8.14 GHz), L2 = 2.93 mm (11.4 GHz), L3 = 1.79 mm (17.1 GHz)

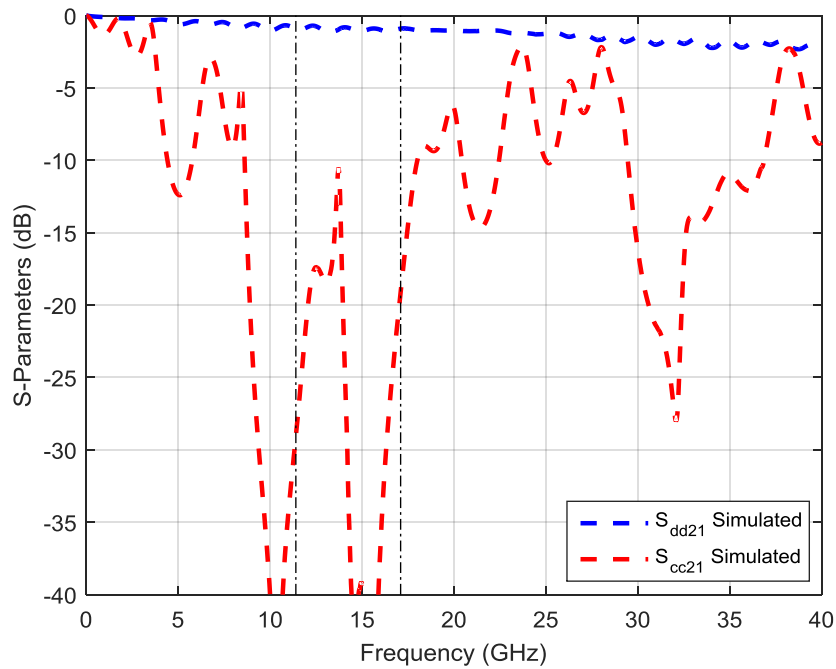


Fig. C.15 - Two cascaded symmetric filters with quarter wavelengths L1 and L2.
 L1 = 2.93 mm (11.4 GHz), L2 = 1.79 mm (17.1 GHz)

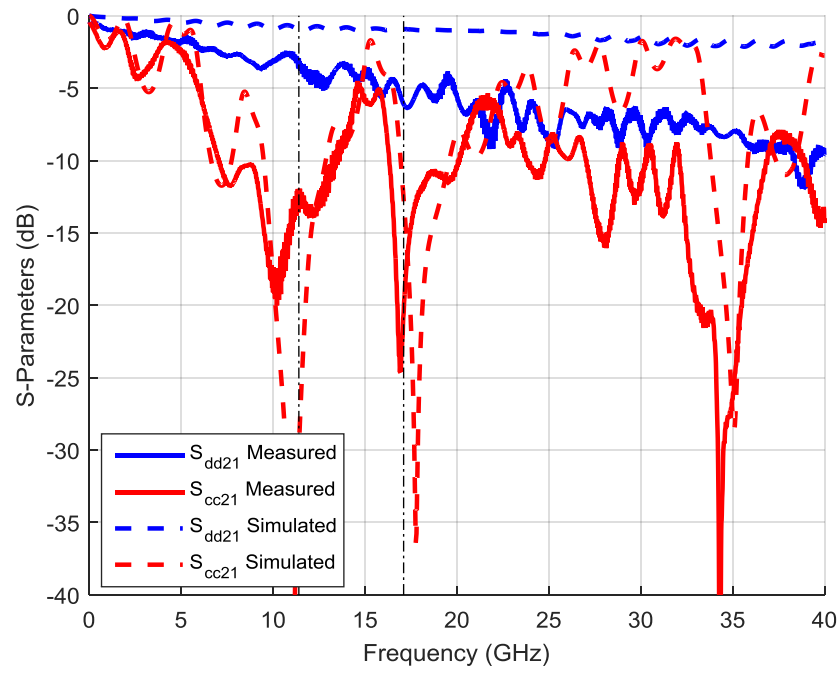


Fig. C.16 - Single asymmetric filter with quarter wavelengths L1 and L2.
L1 = 2.93 mm (11.4 GHz), L2 = 1.79 mm (17.1 GHz)